Rapid-Update Radar Observations of Downbursts Occurring within an Intense Multicell Thunderstorm on 14 June 2011

CHARLES M. KUSTER

Cooperative Institute for Mesoscale Meteorological Studies, and NOAA/OAR/National Severe Storms Laboratory, and University of Oklahoma, Norman, Oklahoma

PAMELA L. HEINSELMAN

NOAA/OAR/National Severe Storms Laboratory, and University of Oklahoma, Norman, Oklahoma

TERRY J. SCHUUR

Cooperative Institute for Mesoscale Meteorological Studies, and NOAA/OAR/National Severe Storms Laboratory, and University of Oklahoma, Norman, Oklahoma

(Manuscript received 25 June 2015, in final form 17 March 2016)

ABSTRACT

On 14 June 2011, an intense multicell thunderstorm produced one nonsevere and three severe downbursts within 35 km of the rapid-update, S-band phased array radar (PAR) at the National Weather Radar Testbed in Norman, Oklahoma, and the nearby polarimetric research Weather Surveillance Radar 1988-Doppler (KOUN). Data collected from these radars provided the opportunity to conduct a quantitative analysis of downburst precursor signature evolution depicted by 1-min PAR data and the associated evolution of differential reflectivity Z_{DR} depicted by 5-min KOUN data. Precursors analyzed included descent of the reflectivity core, evolution of the magnitude and size of midlevel convergence (i.e., number of bins), and descending ''troughs'' of Z_{DR}. The four downbursts exhibited midlevel convergence that rapidly increased to peak magnitude as the reflectivity core (65-dBZ isosurface) bottom and top descended. The Z_{DR} troughs seen in the 5-min KOUN data appeared to descend along with the core bottom. Midlevel convergence size increased to a peak value and decreased as the reflectivity core descended in the three severe downbursts. In contrast, midlevel convergence size exhibited little change in the nonsevere downburst. The time scale of trends seen in the PAR data was 11 min or less and happened several minutes prior to each downburst's maximum intensity. These results point to the importance of 1-min volumetric data in effectively resolving the evolution of downburst precursors, which could be beneficial to forecast operations.

1. Introduction

As a result of many observational and numerical weather prediction studies, much is known about downbursts (e.g., Fujita and Byers 1977; Fujita and Wakimoto 1983; Straka and Anderson 1993; Wakimoto 2001) and the environments that typically support them (e.g., Caracena et al. 1983; Srivastava 1985; Atkins and Wakimoto 1991). Wilson et al. (1984) used radar observations to define a downburst as any near-surface divergent signature with a velocity differential (hereafter DeltaV) of $10\,m\,s^{-1}$ or higher. To aid in our ability to forecast downbursts, previous radar-based studies (e.g., Isaminger 1988; Wakimoto and Bringi 1988; Roberts and Wilson 1989; Smith et al. 2004) identified downburst precursor signatures that tend to develop prior to damaging winds at the surface. These signatures include descending reflectivity cores (DRCs) and midlevel radial convergence (hereafter midlevel convergence) observed by Isaminger (1988) in Tennessee and Alabama and Roberts and Wilson (1989) in Colorado. Many radar-based studies (e.g., Eilts 1987; Isaminger 1988; Wakimoto and Bringi 1988; Mahale et al. 2013) used relatively slow (3–5 min) volumetric update times, which prevented them from observing trends in precursor evolution. Therefore, they identified precursor signatures or focused

Corresponding author address: Charles M. Kuster, National Weather Center, 120 David L. Boren Blvd., Norman, OK 73072.
E-mail: charles.kuster@noaa.gov

DOI: 10.1175/WAF-D-15-0081.1

on their characteristics rather than quantifying precursor evolution. An exception is Roberts and Wilson (1989), who used 2.0–2.5-min volumetric data collected during the Joint Airport Weather Studies Project (McCarthy et al. 1982) to produce time–height trends of DRCs and midlevel convergence for several downburst-producing storms in Colorado. However, they did not examine trends relative to near-surface downburst evolution (e.g., intensification) or look at differences between severe and nonsevere downbursts.

To address the need for rapid sampling of severe weather, including downbursts, the National Severe Storms Laboratory and partners developed the National Weather Radar Testbed Phased Array Radar (NWRT PAR; hereafter PAR) in Norman, Oklahoma (Forsyth et al. 2005). Heinselman et al. (2008) took advantage of PAR's rapid (1 min or less) volumetric update time to study several severe thunderstorms, including one that produced a severe downburst (i.e., winds 25 m s^{-1} or higher). They observed rapid evolutions of downburst precursor signatures, including a reflectivity core that elongated and descended in only 7 min (i.e., a DRC) and midlevel convergence that developed in association with the DRC. Newman and Heinselman (2012) also observed the elongation and rapid descent of a reflectivity core prior to a damaging downburst associated with a quasi-linear convective system. Mobile radars also provide an opportunity to observe downburst-producing storms with faster volumetric update times, but most mobile-radar studies have focused on supercells and tornadoes. Those that did observe downbursts examined snapshots of precursor evolution rather than observing precursor trends (Vasiloff and Howard 2009) or investigated characteristics of low-level downburst evolution (Willingham et al. 2011).

Other studies (e.g., Caracena et al. 1983; Srivastava 1985, 1987; Proctor 1988, 1989) found that microphysical processes such as melting and evaporation contribute to downdraft intensity. Dual-polarization radar provides a means for observing these processes as well as additional downburst precursor signatures. The ability to observe hail below the environmental melting layer was first recognized by Bringi et al. (1984, 1986) when they identified a dual-polarization radar signature consisting of a very narrow (<1 km in the horizontal) area of near-zero differential reflectivity Z_{DR} completely surrounded by large positive values of Z_{DR}. Wakimoto and Bringi (1988) observed this feature descending to the surface in association with damage caused by a downburst and called it a Z_{DR} hole. Later, vertical cross sections taken through Z_{DR} holes revealed depth to this feature and were called Z_{DR} troughs (e.g., Scharfenberg 2003). Given that this signature can accompany downbursts (e.g., Wakimoto and Bringi 1988; Zrnić et al. 1993; Scharfenberg 2003) and is indicative of downward transport of hail potentially in a downdraft (e.g., Ryzhkov et al. 2013a), it provides a possible precursor to downburst occurrence. For a thorough review of the dual-polarization variables and their applications, the reader is referred to the previous literature (e.g., Herzegh and Jameson 1992; Straka et al. 2000; Ryzhkov et al. 2005; Chandrasekar et al. 2013; Kumjian 2013).

More recent work by Ryzhkov et al. (2013a) and Kumjian et al. (2014) used microphysical models to simulate dual-polarization radar signatures such as the Z_{DR} hole and Z_{DR} column—an area of positive Z_{DR} located above the environmental melting layer (e.g., Caylor and Illingworth 1987; Kumjian and Ryzhkov 2008). Kumjian et al. (2014) found that as the updraft weakened and hail began to fall, the Z_{DR} column dissipated and a Z_{DR} hole developed. Furthermore, Ryzhkov et al. (2013a) reported that the depth of the Z_{DR} hole was related to downdraft velocity. Based on these model results, Z_{DR} columns and holes could be useful signatures for anticipating hail and downbursts at the surface if their evolution is adequately sampled.

Single- and dual-polarization precursor evolution is challenging to sample with operational radar-update times of 4–5 min because these signatures typically evolve over time scales of less than 10 min (e.g., Wakimoto and Bringi 1988; Roberts and Wilson 1989; Heinselman et al. 2008). This rapid evolution limits our understanding of precursor trends. Fortunately, rapid-update PAR data provide a more complete evolutionary picture of precursor signatures and their time scales (Heinselman et al. 2008; Newman and Heinselman 2012), but radar studies have not quantified precursor trends relative to the development and intensification of downbursts. Therefore, the purpose of this study is to use 1-min volumetric PAR data to quantify trends in radar-based precursors relative to the onset and maximum intensity of several downbursts produced by a multicell thunderstorm that developed in central Oklahoma on 14 June 2011. These precursors include DRCs and midlevel convergence observed by PAR, and Z_{DR} troughs observed by the nearly collocated research Weather Surveillance Radar 1988-Doppler (WSR-88D; KOUN). The Z_{DR} troughs are examined to assess their ability to track their evolution with operational scanning strategies and to relate them to the evolution of traditional precursors.

The 14 June 2011 storm is an ideal case for examining downburst precursor evolution because the storm occurred within 50 km of PAR and KOUN and produced severe and nonsevere downbursts. One downburst caused tree damage approximately 35 km west of PAR

and KOUN in Tuttle, Oklahoma, and another was associated with two high-wind reports near Newcastle, Oklahoma, approximately 15 km west of PAR and KOUN (NCDC 2011). It also provided a challenge to forecasters at the Norman National Weather Service (NWS) Forecast Office because the downbursts were more intense than anticipated, and the storm produced downbursts for a prolonged time period (approximately 55 min; D. Speheger, NWS Forecast Office Norman, 2015, personal communication). The storm's approximately 160-min life span also set it apart from isolated downburst-producing storms with typical life spans of 60 min or less (e.g., Eilts 1987; Straka and Anderson 1993; Heinselman et al. 2008). To examine potential reasons for this storm's unique characteristics, the environmental conditions on 14 June 2011 were compared to environments associated with previously studied downbursts (section 3).

2. Radar data

PAR transmits at a wavelength of 9.38 cm (S band) and has a broader transmit beamwidth than the WSR-88Ds. The beamwidth is 1.5° at boresight and increases to 2.1° at ±45° from boresight (Table 1). The radar electronically scans a 90° sector, allowing for approximately 1-min volumetric update times, while electronic beam steering provides adaptive scanning capabilities (Zrnić et al. 2007). The current research radar employs a single panel to scan a 90° sector. A future operational radar system would require four panels to scan the full 360° sector similarly to the current WSR-88D network. On 14 June 2011, PAR radar operators employed a modification of the NWS volume coverage pattern 12 (VCP 12; Brown et al. 2005) that contained an additional five elevation angles up to 52.90°. These additional elevation angles proved useful in tracking deep DRCs (section 5) when the storm was within 30 km of the radar. The Adaptive Digital Signal Processing Algorithm for PAR Timely Scans algorithm (ADAPTS; Heinselman and Torres 2011) was also used, which resulted in varying volume scan update times that ranged from 50 s near storm initiation to 63 s as the storm neared the radar site.

Dual-polarization radar data were collected with KOUN, which transmits at a wavelength of 11.09 cm (S band) and has an effective beamwidth of 0.92° (Table 1). On 14 June 2011, the NWS's Radar Operations Center operated KOUN and utilized a VCP 11 (Brown and Wood 2000) scanning strategy, resulting in 360° volumes being collected approximately every 5 min. Both radars began operating prior to initial storm development at 2257 UTC 14 June 2011. The data analysis period for both radars ended at 0024 UTC 15 June 2011, which was just prior to an intense downburst that produced a damaging thunderstorm wind gust (31 m s^{-1}) that knocked out power at the PAR site.

TABLE 1. Overview of PAR and KOUN specifications on 14 Jun 2011.

	PAR	KOUN
Wavelength	9.38 cm	11.09 cm
Transmit beamwidth	1.5° (2.1° at ±45° from boresight)	0.92°
Transmit power	750 kW	750 kW
Range sampling	240 m	250 m
14 Jun 2011 update time	50–63 s	5 min
Beam steering	Electronic	Mechanical

3. Storm environment

On 14 June 2011, atmospheric conditions appeared favorable for strong thunderstorms potentially capable of producing downbursts. At 2207 UTC, just prior to storm initiation, an analysis of surface conditions showed a stationary front draped across portions of central Oklahoma (Fig. 1). This boundary aided in thunderstorm development including an intense downburst-producing multicell storm (see section 4 for details of storm evolution). The 0000 UTC 15 June 2011 Norman sounding (Fig. 2a), launched near the time of storm development, contained temperature and moisture profiles that were consistent with previous wet downburst studies (e.g., Eilts and Doviak 1987; Atkins and Wakimoto 1991; Straka and Anderson 1993). An ''inverted V'' shape in the lowest 300 hPa, higher relative humidities than those observed in dry downburst soundings (e.g., Caracena et al. 1983; Wakimoto 1985), and a deep moist layer at midlevels indicated a potentially favorable environment for wet downbursts. In particular, numerical simulations conducted by Srivastava (1985) indicated that higher environmental relative humidities, like those observed on 14 June 2011, allowed for greater differences between the virtual temperature of the downdraft and its surrounding environment, thereby increasing the downdraft's negative buoyancy.

The height of the environmental melting level and wet-bulb zero height also affects the potential for wet downbursts (e.g., Proctor 1989; Ryzhkov et al. 2013a,b). On 14 June 2011, the environmental melting level and wet-bulb zero height resided near 4.5 and 3.5 km above ground level, respectively, providing a deep layer for potential melting of ice-phase hydrometeors. This deep layer was likely important for downburst formation because previous studies have shown that melting is

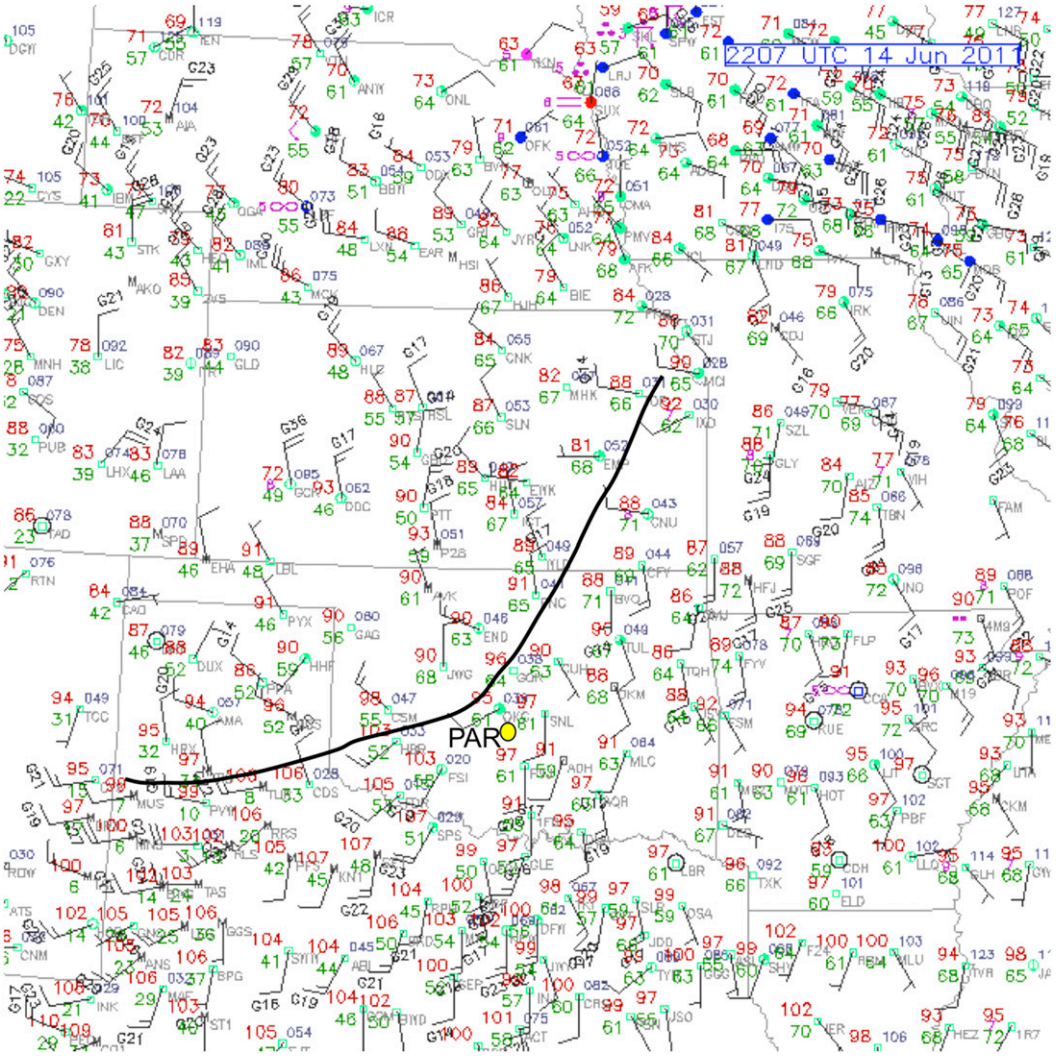

FIG. 1. Surface observations at 2207 UTC 14 Jun 2011 annotated with the subjectively identified location of the stationary front (black line) and PAR (yellow circle). Station surface observations are temperature (°F, red), dewpoint temperature (°F, green), pressure (hPa, blue), wind speed and direction (full barb = 10 kt, where 1 kt = 0.51 m s^{-1}), and gusts (gray "G"). (Data taken from the UCAR image archive; available online at http://www.mmm.ucar.edu/imagearchive/.)

especially important for generating downbursts in an environment with higher relative humidities (e.g., Srivastava 1987; Proctor 1988; Atkins and Wakimoto 1991). The sounding analysis also revealed high instability (CAPE of 2151 J kg^{-1}) and moderate vertical wind shear that was favorable for strong updrafts and organized storm modes capable of supporting large hail growth (e.g., Fawbush and Miller 1953; Nelson 1983; Jewell and Brimelow 2009). This potential for hail was important because Straka and Anderson (1993) found that, in environments conducive for wet downbursts, simulated downdrafts with melting ice-phase hydrometeors were twice as strong as simulated downdrafts with only evaporating raindrops.

The primary difference between the 0000 UTC 15 June 2011 sounding and many previously examined wet downburst soundings (e.g., Atkins and Wakimoto 1991) was the increased vertical wind shear (Fig. 2b). The 0000 UTC 15 June 2011 500-hPa chart (Fig. 3) contained a short-wave trough centered over western Oklahoma. This trough was responsible for moderately strong southwesterly flow of 25 m s^{-1} over central Oklahoma. For comparison, all wet downburst cases examined by Atkins and Wakimoto (1991) had 500-hPa flow of 10 m s^{-1} or less (Fig. 2b). The vertical wind shear and 500-hPa flow were similar to a study of hybrid multicell–supercell storms by Nelson (1987) where mid- and upper-level winds were 25 m s^{-1} or higher. In this case,

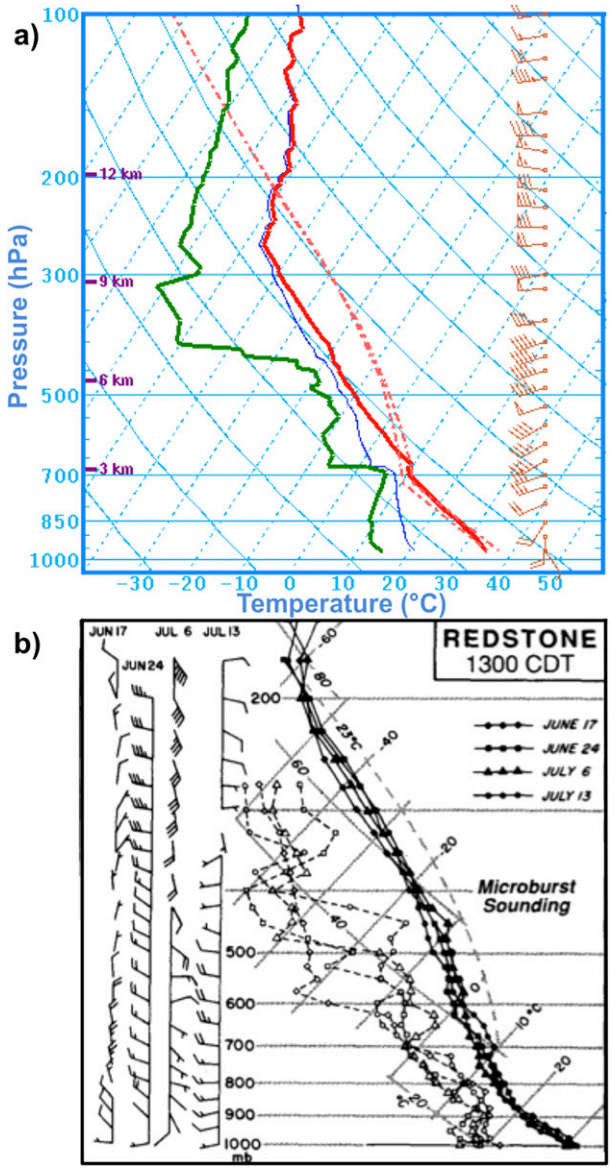

FIG. 2. (a) The 0000 UTC 15 Jun 2011 Norman sounding obtained from the Storm Prediction Center and (b) soundings taken at 1800 UTC on days with wet downbursts observed by Atkins and Wakimoto (1991) in AL. In (a), red line is temperature, green line is dewpoint temperature, blue line is wet-bulb temperature, and dashed pink lines indicate the temperature of a rising parcel of air with and without the virtual temperature correction. Wind speed and direction (full barb=10 kt) are shown at right in (a) and at left in (b).

increased vertical wind shear supported a long-lived, organized thunderstorm complex that produced widespread hail. The 0000 UTC 15 June 2011 sounding also contained a deeper well-mixed dry layer than many soundings associated with wet downbursts in the southeast United States (e.g., Atkins and Wakimoto 1991; Fig. 2b). The sounding appeared more similar to wet downburst soundings in Colorado (e.g., Hjelmfelt 1987; Kessinger et al. 1988) and Arizona (Vasiloff and Howard 2009). Therefore, the environment of 14 June 2011 appeared favorable for organized thunderstorms (i.e., multicells or supercells) capable of producing severe weather, including wet downbursts. The longevity of the downburst-producing storm that ultimately developed did place it near the upper bound of storm severity anticipated by NWS forecasters (D. Speheger, NWS Forecast Office Norman, 2015, personal communication).

4. Storm evolution

During the afternoon hours of 14 June 2011, several short-lived, weak storms developed west of PAR prior to intense convective activity (Fig. 4a). At 2254:14 UTC, the first reflectivity echo (i.e., 20 dBZ or higher at any elevation angle) associated with the downburst-producing storm was detected by PAR just south of the stationary front (Figs. 1 and 4a). The storm intensified over the next 22 min and developed reflectivities $\geq$ 50 dBZ by 2309:32 UTC and $\geq$ 65 dBZ by 2316:40 UTC (Figs. 4b,c). Hereafter, the storm complex continued to grow and by 2343:13 UTC, two storms—evidenced by two distinct reflectivity cores—were evident (Figs. 4d,e). The northern storm moved northeastward toward Oklahoma City, Oklahoma, while the southern storm moved eastward toward Norman. This southern storm is the focus of our study.

The southern storm began to rapidly intensify at approximately 2330:55 UTC, and by 2341:17 UTC had developed evidence of broad midlevel rotation. A small Z_{DR} column had also developed by this time (2330:08 UTC; Fig. 5a), marking the updraft location (e.g., Hall et al. 1984; Brandes et al. 1995). The 1.0-dB isosurface within the Z_{DR} column was used to determine the Z_{DR} column height. At 2330:08 UTC the Z_{DR} column height extended to ~5.3 km above radar level (ARL; hereafter all heights are ARL), or ~0.8 km above the environmental melting layer, and was located just south of the highest reflectivities. The Z_{DR} column briefly grew to a height of ~6.4 km at 2335:08 UTC as the reflectivity core grew upward, but in general its maximum height remained near 5.0 km. By 2342:35 UTC, maximum reflectivity values had increased to 70 dBZ at a height of 8.3 km while the Z_{DR} column had grown in size (Fig. 5b) and continued to have a maximum height of about 5.0 km. This increase in Z_{DR} column size indicated an increase in updraft strength and a potential for increased surface precipitation intensity—including large hail (e.g., Picca et al. 2010; Kumjian et al. 2014). As a result of this strengthening updraft, the reflectivity core continued to expand vertically and horizontally. By 2354:41 UTC, an expansive area of very high reflectivity (60–75 dBZ)

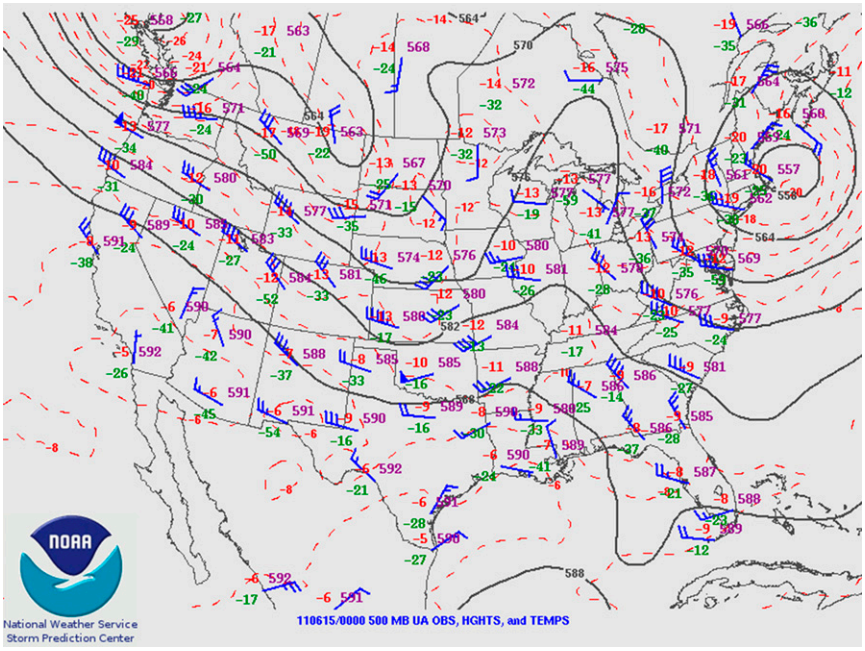

FIG. 3. The 0000 UTC 15 Jun 2011 500-hPa chart obtained from the Storm Prediction Center. Dark lines are isohypses, dashed red lines are isotherms, red numbers are temperature (°C), and green numbers are dewpoint temperature (°C).

existed aloft and a clear three-body scatter spike (TBSS; e.g., Wilson and Reum 1986) had developed (Figs. 4e–g and 5b,c). Analysis of dual-polarization data showed near-zero Z_{DR} values collocated with high reflectivity (Fig. 5c). These signatures indicated lofted hail, which could increase downdraft intensity via melting—if hail fell below the environmental melting level—and hydrometeor loading (e.g., Nelson 1987; Ryzhkov et al. 2013a,b; Richter et al. 2014).

The NWS responded to this intensification by issuing the first severe thunderstorm warning for the storm at 2359 UTC. Six minutes after warning issuance and 71 min after initial storm development, a downburst produced tree damage in Tuttle at 0005 UTC 15 June 2011 (NCDC 2011). Large hail (3.8 cm) was also reported just east of Tuttle several minutes later (0013 UTC; NCDC 2011), which confirmed radar-based evidence of hail within the thunderstorm (Fig. 5c). After the downburst in Tuttle, the storm continued to intensify (Figs. 4g,h) and produced four more downbursts, including two severe downbursts, from 0005 to 0021 UTC, before PAR data collection ceased. Thereafter, the storm produced a severe downburst in Norman that resulted in widespread tree and power line damage. This downburst was not included in this study because PAR data were not available because of disruptions to the power grid. The storm later dissipated approximately 60 km east of Norman at around 0147 UTC.

The storm on 14 June 2011 exhibited different characteristics than most wet downburst-producing storms in the central and southeastern United States analyzed in previous studies (e.g., Eilts 1987; Ellrod 1989; Atkins and Wakimoto 1991). PAR and KOUN detected maximum reflectivities up to 74 dBZ, which were higher than other wet downburst-producing storms that typically have maximum reflectivities < 65 dBZ (e.g., Eilts 1987; Wakimoto and Bringi 1988). The 14 June 2011 storm also took longer than normal to produce the first downburst (65 min from first echo), but then continued to produce downbursts for approximately the next 55 min. Most storms considered in previous studies produced downbursts between 10 and 35 min after storm initiation (e.g., Wakimoto and Bringi 1988; Ellrod 1989; Knupp 1996; Vasiloff and Howard 2009). Frequently, the storms would weaken after producing the first downburst, though the longer-lived multicellular storms studied by Vasiloff and Howard (2009) and Knupp (1996) produced downbursts for approximately 46 and 90 min, respectively.

5. Radar data analysis of downburst precursor signatures

Analysis of the 14 June 2011 storm focuses on radar-based downburst precursor signatures (e.g., Wilson et al. 1984; Isaminger 1988; Roberts and Wilson 1989). In a study of 34 downbursts in Alabama and Tennessee,

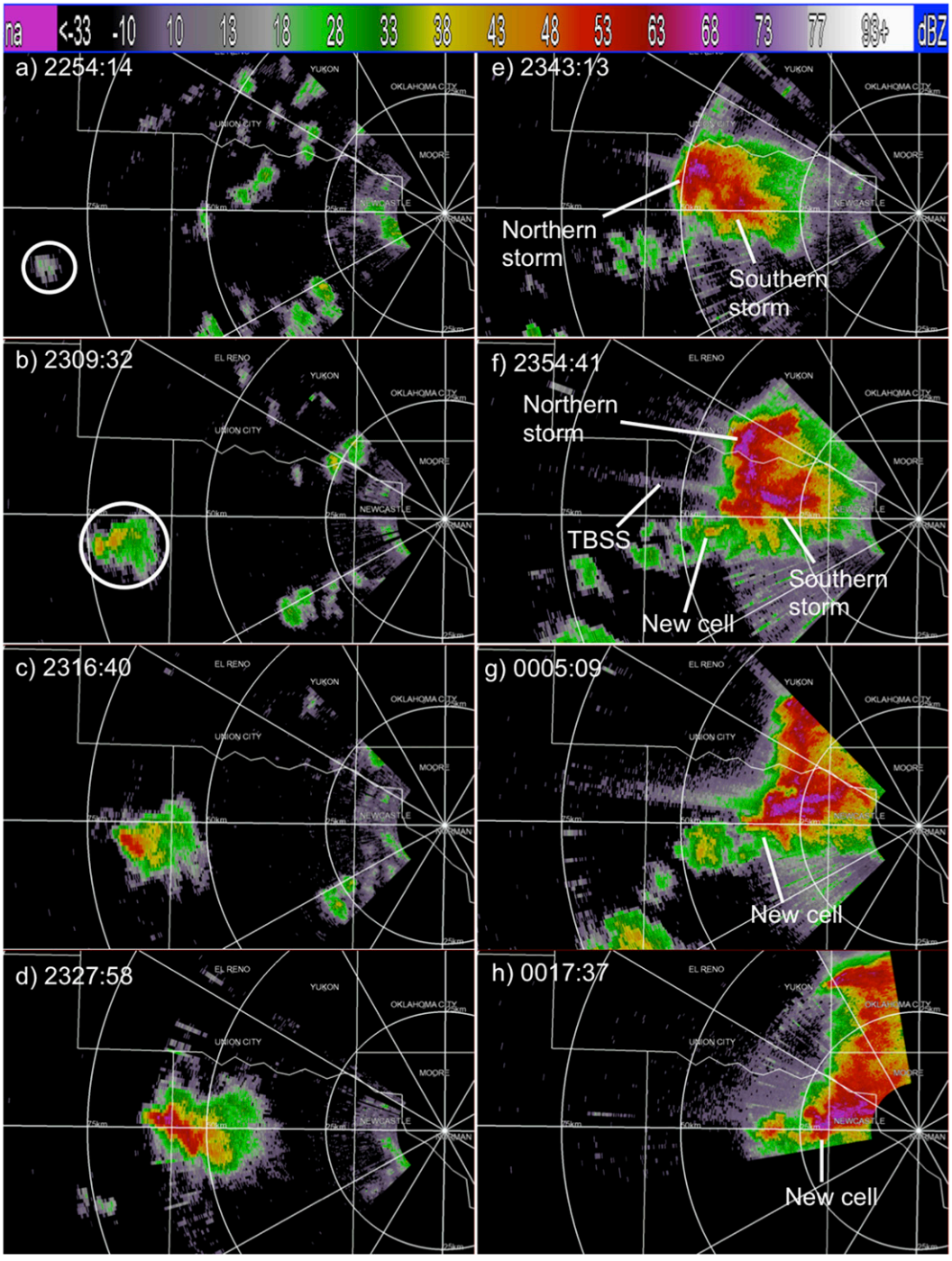

FIG. 4. PAR 5.10° reflectivity depicting storm evolution at (a) 2254:14, (b) 2309:32, (c) 2316:40, (d) 2327:58, (e) 2343:13, (f) 2354:41, (g) 0005:09, and (h) 0017:37 UTC 14–15 Jun 2011. White rings indicate range from the radar in 25-km increments, and white lines are azimuth angles from the radar in 30° increments. The storm of interest is marked by the white circles in (a) and (b).

Isaminger (1988) observed a DRC with 95% of the downbursts and midlevel convergence with 41% of the downbursts. In a similar study of 31 downbursts in Colorado, Roberts and Wilson (1989) observed a DRC with 88% of the downbursts, where data were sufficient, and convergence near or above cloud base in 97% of the downbursts. The difference in convergence frequency between Isaminger (1988) and Roberts and Wilson

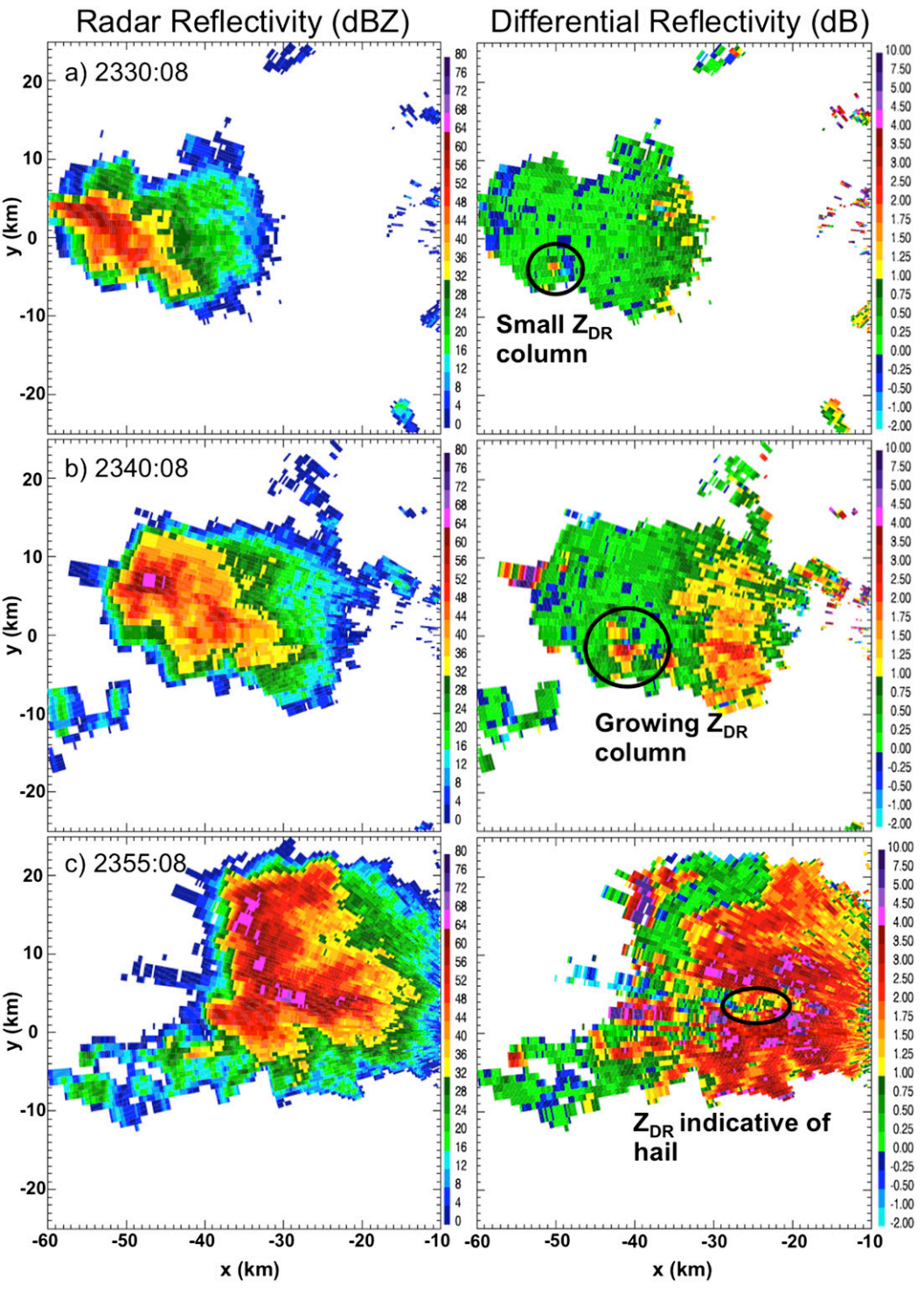

FIG. 5. KOUN (left) Z and (right) Z_{DR} fields at 5.25°-elevation angle showing evolution of the Z_{DR} column and Z_{DR} field associated with southern storm at (a) 2330:08, (b) 2340:08, and (c) 2355:08 UTC 14 Jun 2011. Approximate beam heights at the feature of interest are 5.0 km in (a), 4.0 km in (b), and 2.8 km in (c). Black circles highlight the Z_{DR} column of note.

(1989) may have arisen from differences in radar scanning strategies, radar viewing angle, or environmental characteristics. DRCs and midlevel convergence were also observed prior to downburst development in Oklahoma (e.g., Eilts 1987), Alabama (Straka and Anderson 1993), and Arizona (Vasiloff and Howard 2009), making them the most reliable precursor signatures, especially when observed together (e.g., Isaminger 1988; Schmocker et al. 1996; Smith et al. 2004). The radar analysis in this section focuses on documenting the trends and time scales of DRCs and midlevel convergence associated with each downburst.

To be consistent with previous studies (e.g., Isaminger 1988; Roberts and Wilson 1989), any reflectivity core that developed at an altitude of at least 5 km, descended to the surface, and corresponded with a near-surface (i.e., 0.5°) divergent signature (Fig. 6) was identified as a DRC. Once identified using PAR data, a series of vertical cross sections reconstructed from the plan position indicator (i.e., conical) scans were used to track the minimum and maximum heights of the 65 dBZ isosurface over time. Although several factors, including precipitation fallout occurring without a downdraft, can result in a DRC, we use DRCs—especially when collocated with radial convergence—as a proxy for downdraft location in this study (e.g., Peterson 1984; Roberts and Wilson 1989; Straka and Anderson 1993).

The storm's midlevels were defined as the region between 2 and 6 km ARL (e.g., Eilts et al. 1996). A 1-km buffer was added to each side of this range to ensure that any potential convergence just above or below the midlevel downdraft was captured in the analysis. Therefore, measurements of midlevel convergence magnitude consisted of averaging values of the linear least squares derivatives (LLSD) divergence field (e.g., Smith and Elmore 2004; Newman et al. 2013) associated with each downburst's DRC at all elevation angles with beam heights between 1.0 and 7.0 km. A similar technique was used to quantify the spatial extent (i.e., size) of the midlevel convergence. Range gates with LLSD divergence field values less than 0.0 (i.e., convergent) were counted at all elevation angles with beam heights between 1.0 and 7.0 km. If the depth of a downburst's near-surface divergent signature exceeded 1.0 km, as was the case with the nonsevere downburst, only elevation angles with beam heights between 1.5 and 7.0 km were included. This vertical depth is somewhat greater than the 1–6-km layer frequently used in previous studies (e.g., Isaminger 1988; Smith et al. 2004), but we still refer to the quantity as "midlevel convergence" to be clear that we are examining the precursor signature used in previous research (e.g., Isaminger 1988; Roberts and Wilson 1989).

Measurements of the PAR-sampled near-surface (i.e., 0.5°; approximately 0.5 km on average) radial velocity (hereafter velocity) field provided information about each downburst's time of development and maximum intensity. Downburst development was identified as the first time when DeltaV across the near-surface divergent signature reached 10 m s^{-1} or higher (e.g., Wilson et al. 1984). Downburst maximum intensity was identified as the time when maximum velocity was sampled by PAR within each downburst's near-surface divergent signature.

Dual-polarization data from KOUN provided a means of observing downburst Z_{DR} trough precursor signatures. Analysis of vertical cross sections of Z_{DR} revealed information about the evolution of each downburst's Z_{DR} trough every 5 min. These 5-min Z_{DR} trough "snapshots" were examined with respect to the evolution of each downburst's DRC and the midlevel convergence seen in corresponding PAR volume scans. In addition, several Z_{DR} columns were observed with the multicell thunderstorm, but did not appear to be a reliable downburst precursor signature because Z_{DR} column growth and decay did not coincide well with downburst development or intensification in this case. The slower update time (5 min) of the dual-polarization KOUN radar data likely limited the ability to observe any potential relationships, however.

a. Severe downbursts

For this study, downbursts with a severe wind report in the National Climatic Data Center (now the National Centers for Environmental Information) publication *Storm Data*, or PAR-observed maximum base velocities (at approximately 0.5 km height on average) of 25 m s^{-1} or higher, were classified as severe. Based on this classification scheme, the right-moving storm analyzed herein produced three severe downbursts and one nonsevere downburst west of Norman between 2358 and 0024 UTC. To organize discussion of the downbursts, a naming scheme was developed that assigned a key of "SD" (short for severe downburst) to all severe downbursts and "NSD" (short for nonsevere downburst) to each nonsevere downburst followed by a letter based on chronological order. Therefore, the first severe downburst received the name SD-a, whereas the first nonsevere downburst received the name NSD-a.

1) SD-A

The first severe downburst (SD-a) contained the most isolated DRC of all downbursts studied herein, which was likely responsible for the clear precursor trends observed. A well-defined 65-dBZ reflectivity core (hereafter core) developed aloft (4.7–5.7 km) at

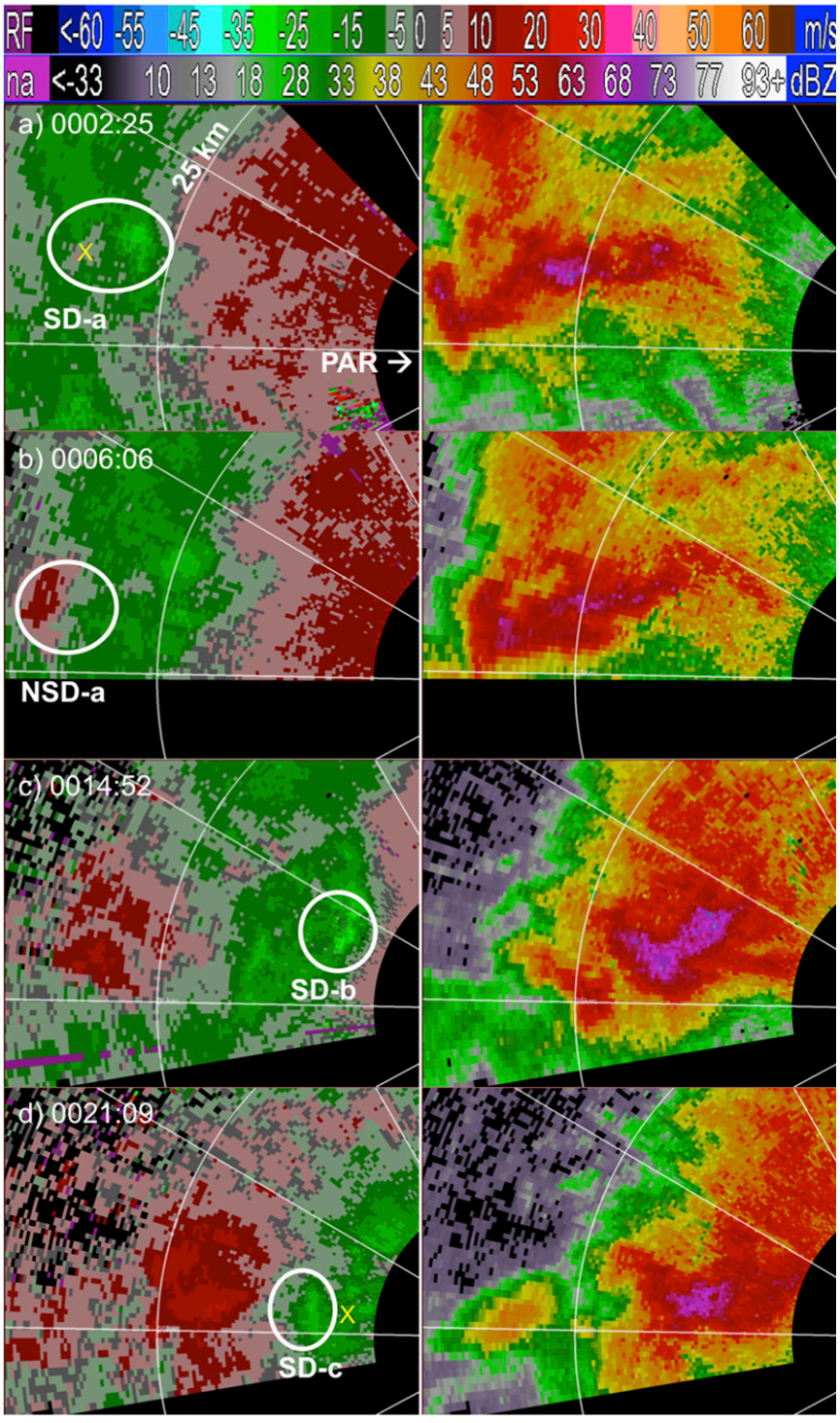

FIG. 6. PAR 0.5° (left) velocity and (right) reflectivity depicting near-surface divergence signatures for (a) SD-a, (b) NSD-a, (c) SD-b, and (d) SD-c at time of downburst maximum intensity (i.e., maximum sampled base velocity). White rings indicate the range from the radar in 25-km increments, and white lines are azimuth angles from the radar in 30° increments. The yellow × marks in (a) and (d) approximate the locations of Tuttle and Newcastle, respectively. Velocity and reflectivity color bars are located at the top.

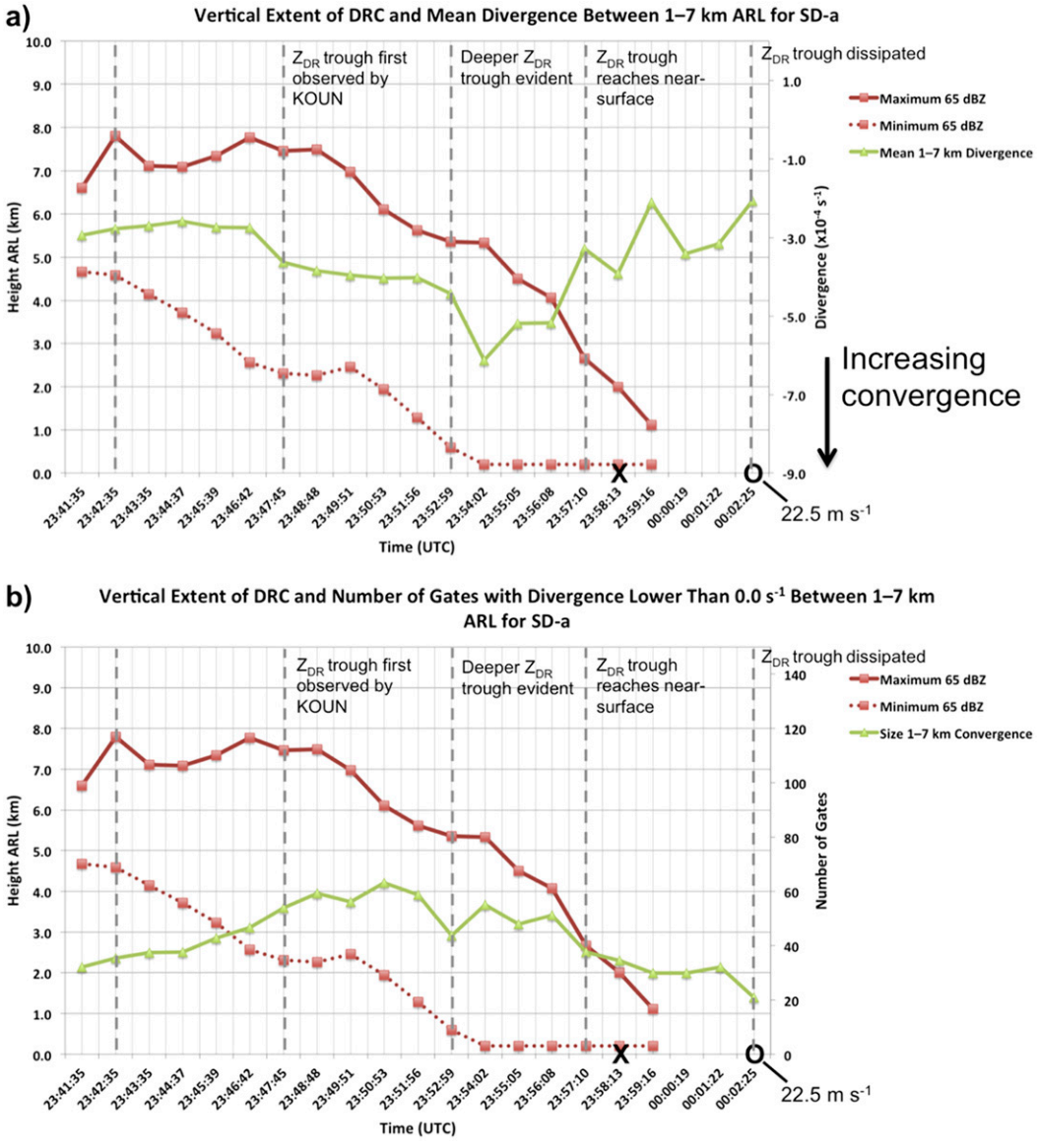

FIG. 7. Evolution of the DRC and the (a) midlevel convergence magnitude and (b) midlevel convergence size associated with SD-a. The solid red line denotes the maximum height of the 65-dBZ isosurface, the dashed red line denotes the minimum height of the 65-dBZ isosurface, and the green line denotes the mean divergence magnitude or size in the 1–7 km ARL analysis layer. In (a), negative divergence is convergence. The time of initial sampling of the near-surface divergent signature is marked by ×, and O marks the time of the downburst's maximum base velocity (annotated). Gray dashed lines indicate the beginning of the corresponding KOUN volume scans and show the evolution of the Z_{DR} trough relative to DRC and the midlevel convergence evolution.

2341:35 UTC, approximately 21 min prior to the downburst's maximum intensity (i.e., maximum base velocity sampled by PAR) at 0002:25 UTC (Fig. 7). Over the next 6 min, it elongated as the core bottom descended to 2.3 km, and the core top remained just below 8.0 km. Midlevel convergence size and magnitude also slowly increased as the core elongated (Figs. 7a,b). Beginning at 2348:48 UTC, the core top began to descend, and the core bottom resumed its descent approximately 1 min later. Midlevel convergence size reached a peak at 2350:53 UTC (Fig. 7b), and midlevel convergence magnitude (Fig. 7a) noticeably increased between 2351:56 and 2354:02 UTC, as the core top and bottom both descended. The observed increases in midlevel convergence size and magnitude were likely the result of air moving inward in response to the deep downdraft

(i.e., theory of mass continuity). After a brief lapse in descent, the core top began continuously and rapidly descending approximately 8 min prior to downburst maximum intensity. It descended approximately 4.2 km in only 5 min and reached a minimum height of 1.1 km at 2359:16 UTC. We suggest that continued collapse of the core top indicated that a downdraft was on going within the storm (e.g., Peterson 1984). Therefore, it was not surprising that descent of the core top occurred just prior to SD-a's maximum intensity (Fig. 7). Additionally, midlevel convergence magnitude and size steadily decreased during this period (2354:02–2359:16 UTC; Figs. 7a,b). We surmise that this decrease in convergence occurred from the overall decrease in core depth, which potentially indicated a decrease in downdraft depth. A shallower and smaller downdraft could be associated with less midlevel convergence, thereby explaining the observed patterns. Approximately 3 min later, at 0002:25 UTC, PAR sampled the maximum base velocity (0.2 km) of 22.5 m s^{-1} associated with SD-a (Fig. 6a). Tree damage was also reported at approximately 0005 UTC (NCDC 2011).

The first KOUN volume scan that sampled SD-a's reflectivity core began at 2342:46 UTC. At this time no Z_{DR} trough was evident, potentially as a result of the reflectivity core residing above the in-storm melting layer (Figs. 7 and 8a). The in-storm melting layer height of 3.4–3.9 km was determined using dual-polarization variables (i.e., Z_{DR} and correlation coefficient) provided by KOUN and is consistent with methods discussed by Giangrande et al. (2008). At the same time (2342:46 UTC), high reflectivity and near-zero Z_{DR} existed at a range of approximately 35 km and a height of 5.5 km (Fig. 8a). These variables suggest that SD-a's reflectivity core consisted of hailstones, which increased the potential downdraft intensity via hydrometeor loading and melting. By the next KOUN volume scan (2347:47 UTC), the reflectivity core had descended below the in-storm melting layer (Figs. 7 and 8b), and a Z_{DR} trough had developed near a range of 33 km (Fig. 8b). Development of this Z_{DR} trough provided further indication that a downdraft was on going in the same location as the DRC observed in the PAR data. The Z_{DR} trough then descended almost in unison with the core bottom observed by PAR over the next 10 min (Figs. 7 and 8c,d) and reached the near surface (0.3 km) at about the same time as downburst development (Fig. 8d, Table 2). Hereafter, the maximum PAR-sampled base velocity (0.3 km) continued to increase through 0002:25 UTC (Fig. 7), and the DRC and Z_{DR} trough dissipated by 0002:46 UTC (Fig. 8e). The downburst probably began weakening shortly thereafter as base velocities continuously decreased and no other damage reports were received after the tree damage occurred in Tuttle at approximately 0005 UTC (NCDC 2011). We infer that DRC and Z_{DR} trough dissipation suggested downdraft weakening (e.g., Ryzhkov et al. 2013a; Kumjian et al. 2014), which likely aided in the downburst dissipation.

2) SD-B

As the storm intensified, a large area of very high reflectivity developed within the storm (Figs. 4f–h). The DRC of SD-b was embedded within this area of high reflectivity, making precursor measurements more challenging than those of SD-a. SD-b's 65-dBZ core developed aloft (2.9–6.3 km) at 2356:08 UTC, approximately 19 min prior to the downburst's maximum intensity (0014:52 UTC; Fig. 9). Similarly to SD-a, the core elongated between 2356:08 and 0003:27 UTC as the core bottom descended and the core top remained near a height of 6.5 km. The midlevel convergence magnitude and size also increased during this time (2356:08–0001:22 UTC; Figs. 9a,b). We suggest that this increase occurred in response to a low-level downdraft potentially associated with descent of the core bottom (e.g., Straka and Anderson 1993; Fig. 9).

Beginning at 0003:27 UTC, rapid growth of the core occurred as the core top grew from a height of approximately 6.3 km at 0003:27 UTC to 9.32 km at 0006:06 UTC (Fig. 9). During this same period, the midlevel convergence magnitude and size decreased slightly (Figs. 9a,b). Hereafter, the core top descended rapidly toward the surface and reached its minimum height of 2.9 km at the same time that PAR sampled the maximum base (0.2 km) velocity of 30.0 m s^{-1} (0014:52 UTC; Figs. 6c and 9). The collapse of the core top occurred approximately 9 min prior to this maximum base velocity (i.e., SD-b's maximum intensity). Additionally, the midlevel convergence size and magnitude increased once again beginning at 0007:09 and 0009:14 UTC, respectively, perhaps in response to the rapid descent of the core top through the storm's midlevels (Figs. 9a,b). Both the midlevel convergence magnitude and size then decreased just after SD-b's maximum intensity at 0014:52 UTC.

The first KOUN volume scan that sampled SD-b's reflectivity core began at 2357:47 UTC. At this time, the core had already descended just below the in-storm melting layer (Fig. 9), and a shallow Z_{DR} trough had developed at a range of about 25 km (Fig. 10a). Over the next 10 min, two KOUN volume scans depicted the descent of the Z_{DR} trough (Figs. 10b,c). It descended along with the core bottom observed by PAR and reached the near surface (0.2 km) at about the same time as the initial downburst development (Figs. 9 and 10c,

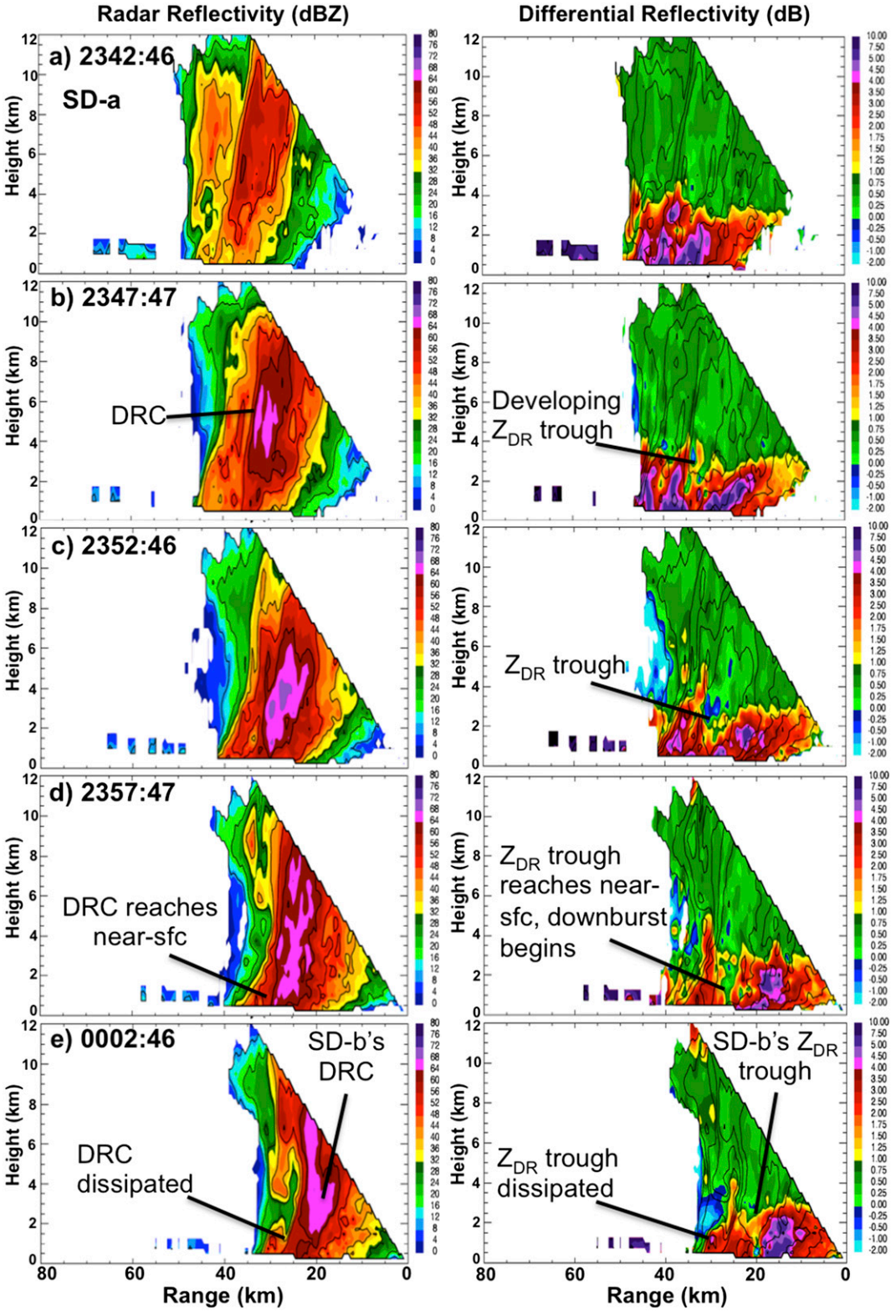

FIG. 8. Vertical cross sections of KOUN (left) reflectivity and (right) differential reflectivity for SD-a at (a) 2342:46, (b) 2347:47, (c) 2352:46, (d) 2357:47, and (e) 0002:46 UTC 14–15 Jun 2011. Azimuths are 271°, 275°, 278°, 281°, and 284°, respectively. KOUN is located in the bottom-right corner of each image. The *y* axis is height (km ARL), and the *x* axis is range from the radar (km). Storm motion is toward the radar, or from left to right. SD-b's unrelated DRC is also noted.

TABLE 2. Overview of downburst names, initial development times (i.e., DeltaV reaches 10 m s^{-1}), storm reports, and maximum downburst intensity (i.e., maximum PAR-sampled base velocity) on 14 Jun 2011. EG is "estimated gust."

Downburst	Time (UTC) when DeltaV reached 10 m s^{-1} or higher	Storm report, time (UTC)	Max base velocity (m s^{-1}), time (UTC)
SD-a	2358:13	Downed tree limbs, 0005	22.5, 0002:25
SD-b	0006:06	None	30.0, 0014:52
SD-c	0018:01	EG 30 m s^{-1}, 0023	22.5, 0021:09
NSD-a	0002:25	None	14.0, 0006:06

Table 2). The Z_{DR} trough was then maintained over the next 5 min as the core top descended (Fig. 10d). Both the reflectivity core and Z_{DR} trough had dissipated by the next KOUN volume scan (0017:46 UTC; Fig. 10e).

3) SD-c

A new storm developed just to the southwest of the primary thunderstorm (Figs. 4g,h) as the latter storm's reflectivity core continued to expand (Figs. 4f–h). A

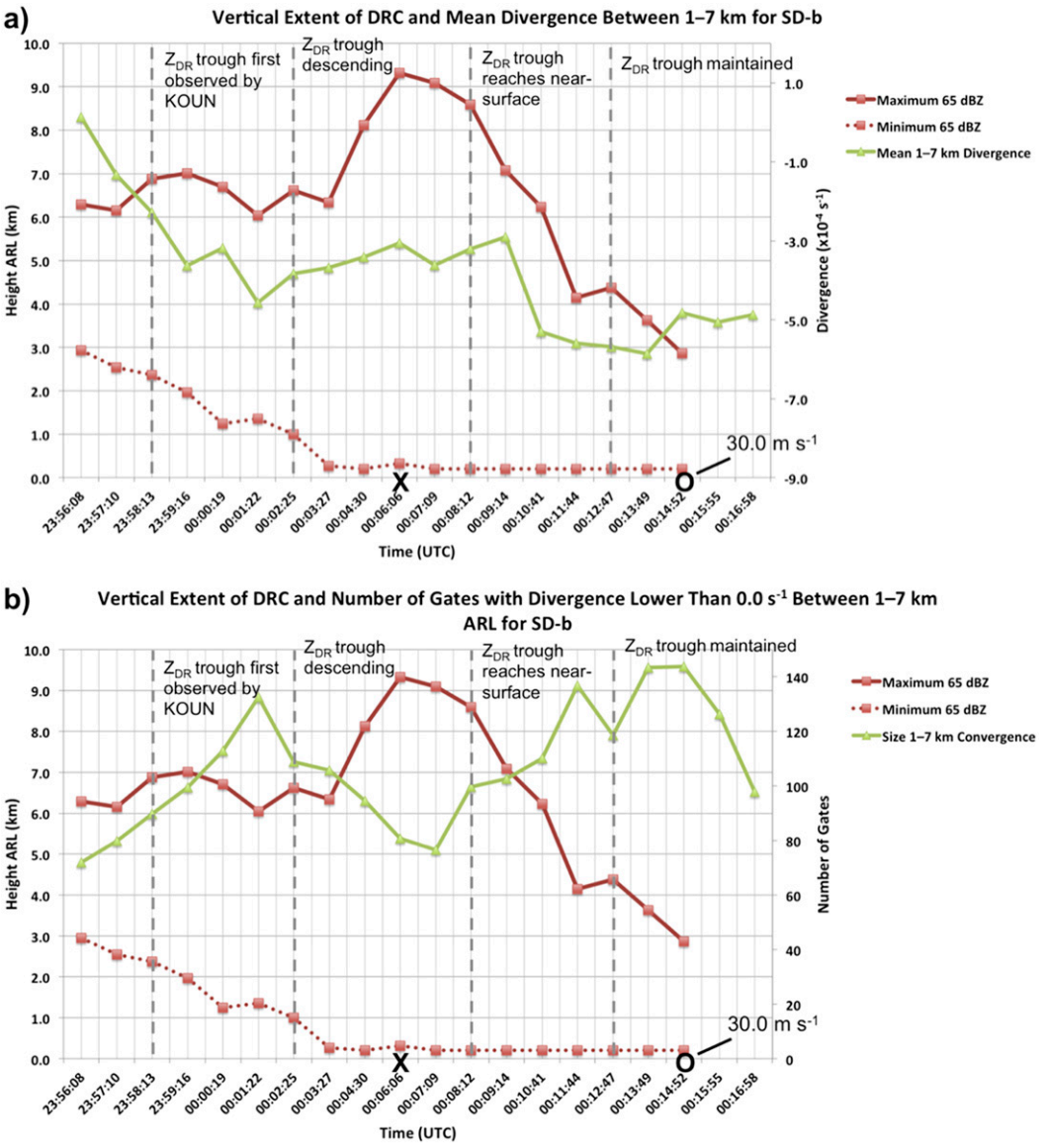

FIG. 9. As in Fig. 7, but for SD-b.

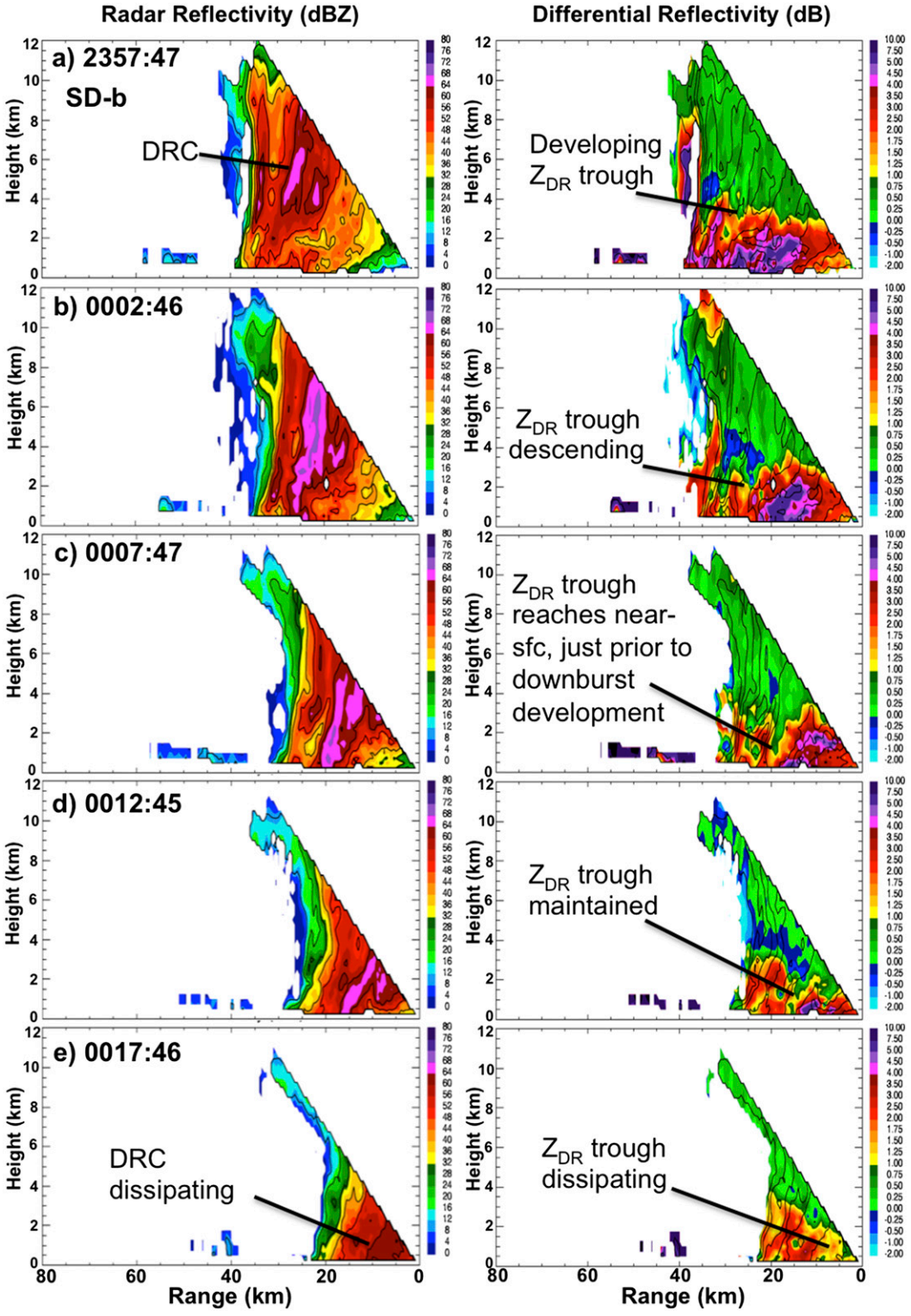

FIG. 10. As in Fig. 8, but for SD-b at (a) 2357:47, (b) 0002:46, (c) 0007:47, (d) 0012:45, and (e) 0017:46 UTC 14–15 Jun 2011. Azimuths are 277°, 281°, 286°, 291°, and 295°, respectively.

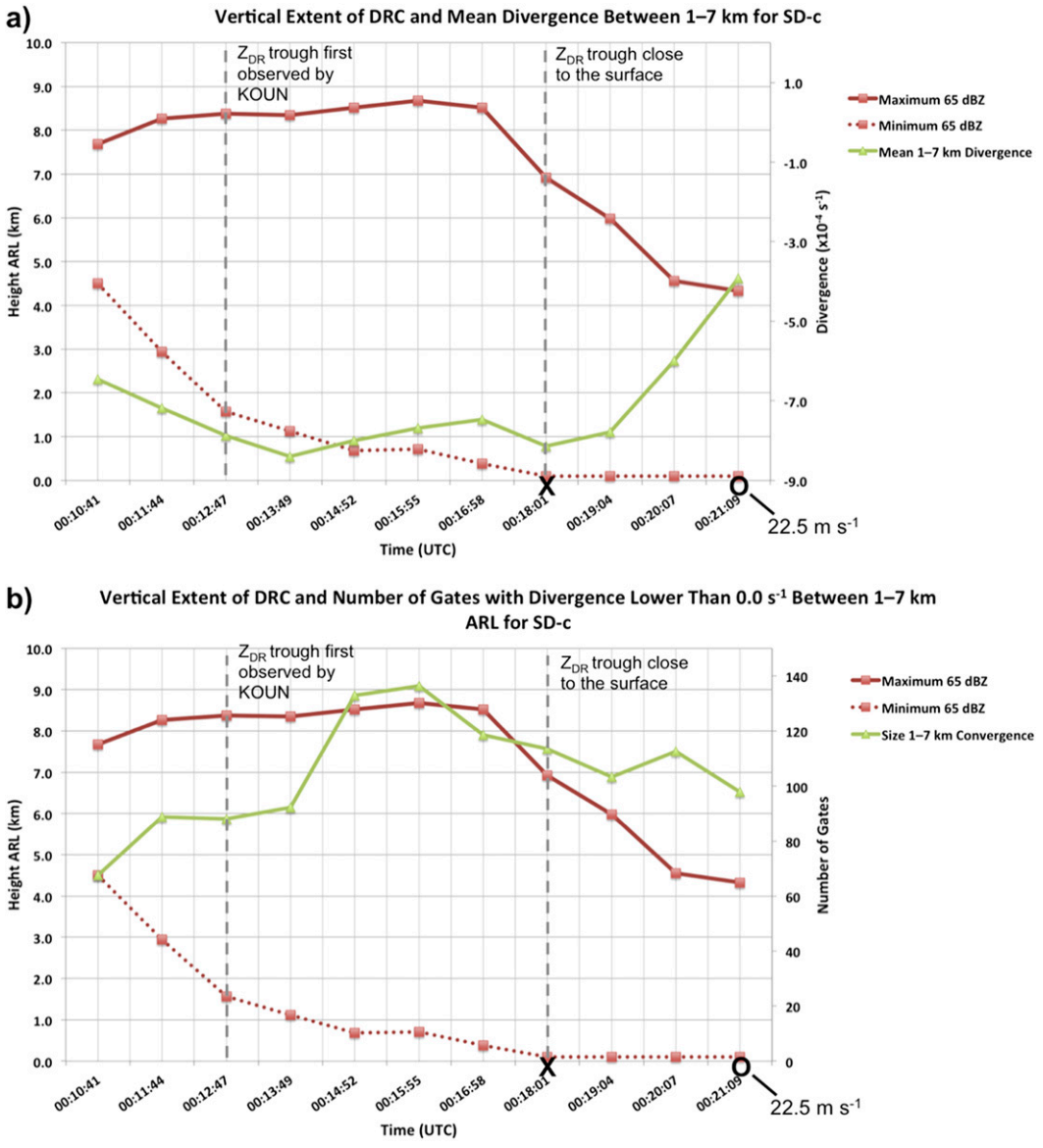

FIG. 11. As in Fig. 7, but for SD-c.

DRC was evident within this new cell as it merged with the primary thunderstorm. This DRC was associated with the development of the third identifiable severe downburst, SD-c. Since PAR data collection ended prior to the near-surface divergent signature of SD-c weakening, it is possible that the time for downburst maximum intensity presented herein is a few minutes later than shown.

The core of SD-c developed aloft (4.2–7.8 km) at 0010:41 UTC, at least 11 min prior to the downburst's maximum intensity at 0021:09 UTC. Similarly to the other severe downbursts, SD-c's core elongated as the core bottom descended to the surface by 0018:01 UTC, while the core top remained near 8.5 km through 0016:58 UTC (Fig. 11). The midlevel convergence magnitude and size also increased between 0010:41 and 0013:49 UTC, potentially in response to the descent of the core bottom, and, by extension, a low-level downdraft (e.g., Straka and Anderson 1993; Figs. 11a,b). At 0016:58 UTC, at least 4 min prior to the downburst maximum intensity, the core top began to rapidly descend. It descended approximately 4.2 km between 0016:58 and 0021:09 UTC and reached a minimum height of 4.3 km. The midlevel convergence size began decreasing at 0015:55 UTC, while the midlevel convergence magnitude remained relatively strong through 0019:04 UTC as

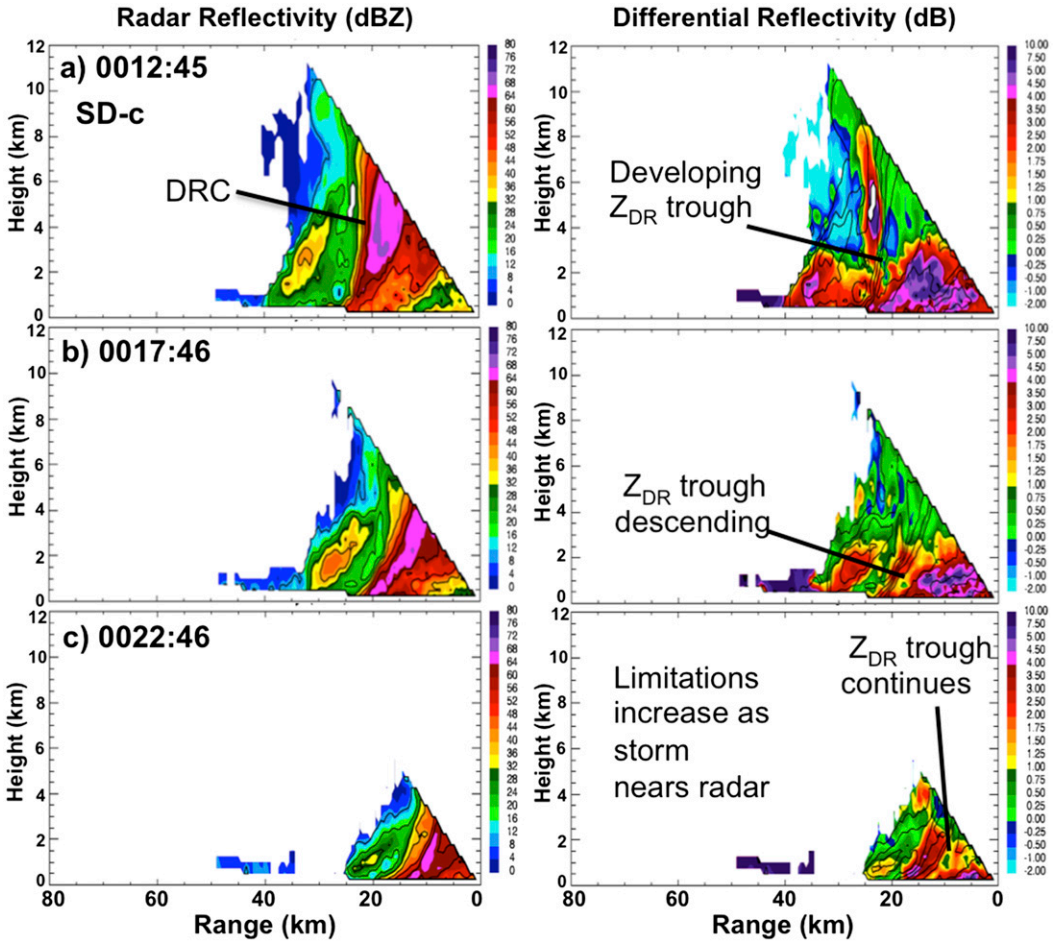

FIG. 12. As in Fig. 8, but for SD-c at (a) 0012:45, (b) 0017:46, and (c) 0022:46 UTC 15 Jun 2011. Azimuths are 272°, 274°, and 280°, respectively.

the core top descended, before it decreased rapidly between 0019:04 and 0021:09 UTC. We suggest that this decrease in convergence magnitude and size potentially resulted from either decreasing downdraft depth, as evidenced by the decrease in core-top height (Figs. 11a,b); intensity; or both. PAR also sampled the maximum base (0.2 km) velocity of 22.5 m s^{-1} at this time (0021:09 UTC, Fig. 6d) and an off-duty NWS employee located near Newcastle experienced the thunderstorm winds and estimated a gust of about 30 m s^{-1} 2 min later at 0023 UTC (NCDC 2011).

The first KOUN volume scan that sampled SD-c's reflectivity core began at 0012:45 UTC. By this time, a large reflectivity core had already developed and a shallow Z_{DR} trough existed at a range of approximately 20 km (Fig. 12a). The Z_{DR} trough and core base (sampled by PAR; Fig. 11) descended over the next 5 min and were near the surface (0.2 km) by the next KOUN volume scan at 0017:46 UTC (Fig. 12b). It was also near this time that SD-c first developed (Table 2). Hereafter, it became increasingly difficult to observe dual-polarization features as the storm moved within 20 km of KOUN. Only portions of the storm below 3 km were sampled at 0022:46 UTC because of the cone-of-silence effect (Fig. 12c). Despite the limitations, it appeared as if SD-c's Z_{DR} trough persisted until at least 0022:46 UTC (Figs. 11 and 12c). By the next KOUN volume scan at 0027:46 UTC (not shown), the reflectivity core and Z_{DR} trough had dissipated. KOUN data also showed that SD-c's maximum base velocities were decreasing, suggesting that the downburst was weakening after 0027:46 UTC. In addition, no storm reports were received in association with SD-c after 0023 UTC when an estimated gust of about 30 m s^{-1} occurred.

b. *Nonsevere downbursts*

For this study, any downburst not meeting the severe criteria outlined in section 5a was classified as

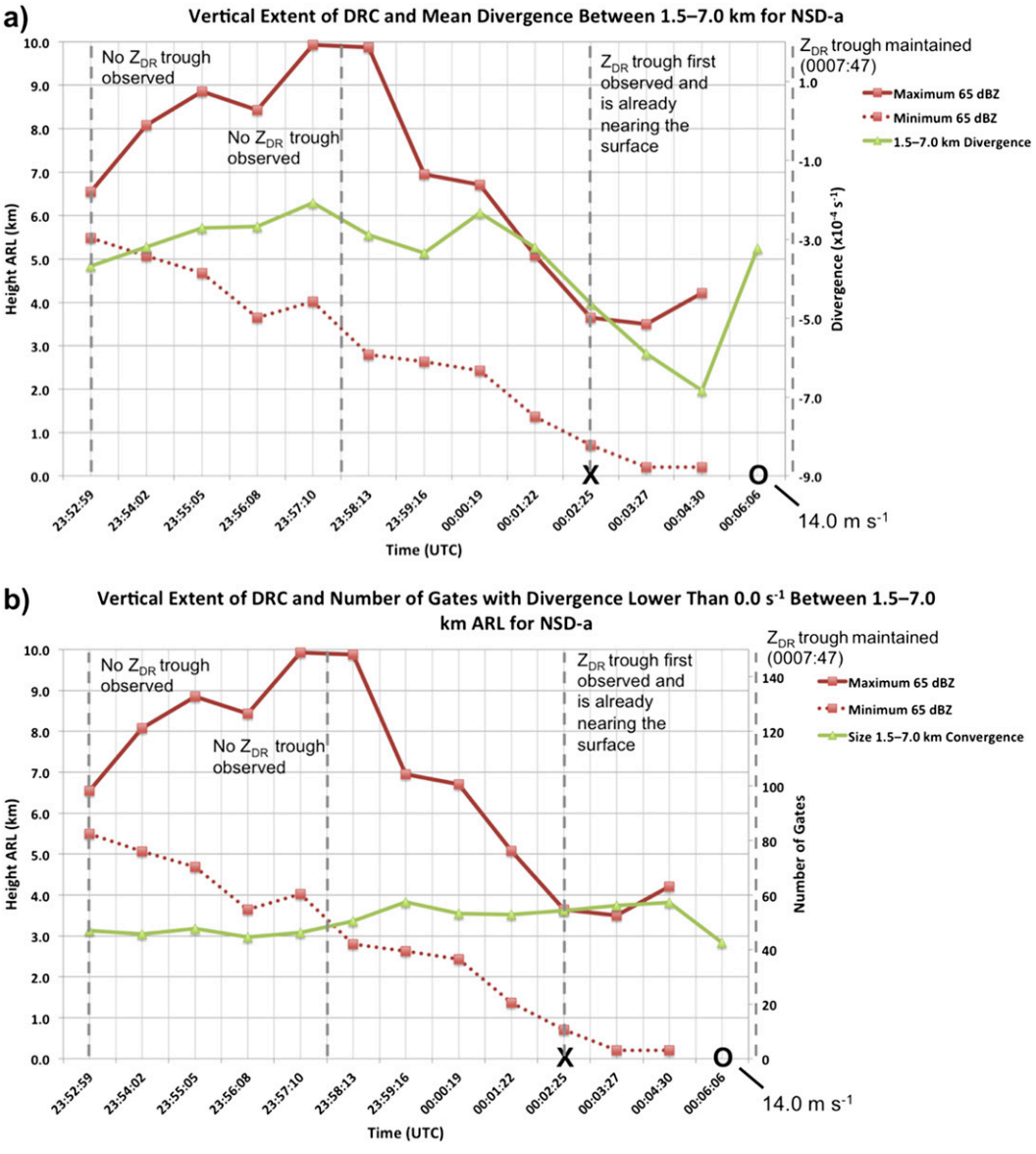

FIG. 13. As in Fig. 7, but for NSD-a.

nonsevere. Only one nonsevere downburst and its precursor signatures were confidently identified with this storm.

NSD-A

NSD-a's core developed aloft (5.5–6.6 km) approximately 13 min prior (2352:59 UTC) to the downburst maximum intensity (Fig. 13). The core elongated through 2358:13 UTC as the core bottom slowly descended, and the core top grew to a height just below 10 km. During this time (2352:59–2358:13 UTC), the midlevel convergence magnitude and size did not noticeably increase. We suspect that these minimal changes occurred because the downdraft was relatively weak and therefore was not associated with strong or spatially large convergence (Figs. 13a,b). Beginning at 2358:13 UTC, approximately 7 min prior to the downburst maximum intensity, the core top collapsed and rapidly descended while the core bottom continued its relatively slow descent. The core top and bottom continued descending until 0003:27 UTC, approximately 1 min after downburst development and 2 min prior to downburst maximum intensity (Table 2), when both reached their minimum heights. It is unclear why DRC evolution differed slightly from the severe downbursts (i.e., the core top and bottom reached their minimum

heights at the same time), but one possible explanation is hydrometeor size. The reflectivity core of NSD-a contained lower (about 4 dBZ) overall reflectivity and a slightly higher (typically 0.93 or higher compared to 0.90 or higher) correlation coefficient than that observed with the severe downbursts. These variables suggest that smaller hail may have existed within NSD-a's reflectivity core. Therefore, it is possible that the decreased descent rate of the core bottom resulted from the lower fall velocity of the smaller hydrometeors.

The midlevel convergence magnitude steadily increased beginning at 0000:19 UTC as descent of the core top and bottom was on going (Fig. 13a). The magnitude continued to increase through 0004:30 UTC, a full 2 min after rapid descent of the core top ended. It is unclear why this increasing trend continued, but perhaps a midlevel downdraft persisted after the core top stopped descending. After reaching its peak magnitude 1 min prior to PAR sampling the maximum base (0.3 km) velocity of 14.0 m s^{-1} (Fig. 6b), the midlevel convergence magnitude quickly decreased for the next minute. We speculate that the low core-top height (3.5 km), and therefore potentially shallow downdraft depth (e.g., Roberts and Wilson 1989), resulted in the sharp decrease in midlevel convergence observed here (Fig. 13a). Despite these changes in midlevel convergence magnitude, the size changed very little and followed a nearly flat-line pattern (Figs. 13a,b).

The first KOUN volume scan that sampled NSD-a's reflectivity core (range of approximately 37 km) began at 2352:46 UTC. Within this core, the existence of near-zero Z_{DR} and relatively high correlation coefficient (>0.96; not shown) values above the in-storm melting layer indicated that hail resided within NSD-a's DRC (Fig. 14a). These hailstones increased the potential downdraft intensity via hydrometeor loading and melting, if the hail melted. The reflectivity core remained above the in-storm melting layer through 2357:47 UTC (Figs. 13 and 14b), so a Z_{DR} trough was not observed until the 0002:46 UTC volume scan (Fig. 14c). By this time, the Z_{DR} trough had already descended to a height of approximately 1 km, which was similar to the core-bottom height observed by PAR (Fig. 13). By the next KOUN volume scan at 0007:47 UTC, NSD-a's reflectivity core had dissipated (not shown).

6. Discussion of precursor signatures

a. Precursor patterns and time scales

The DRCs of all examined downbursts displayed similar evolutionary trends. The core base always began descending prior to the core top (Fig. 15). This evolution is common in thunderstorms as updraft strength tends to be weakest at low levels and accelerates with height as more instability is realized (e.g., Battan and Theiss 1966). This vertical structure of the updraft allows relatively large hydrometeors to fall from low levels first. It was therefore not surprising that the descent of the core top appeared to be more connected to downburst intensification than the descent of the core base on 14 June 2011. For all downbursts, the core top began continuously descending on average 8.6 min prior to the downburst maximum intensity (Table 3), and was always associated with downburst intensification (Fig. 15). We infer that the collapse of the core top was indicative of processes (e.g., precipitation loading) that could result in the development of a strong downdraft. This collapse and descent of the core top also occurred very quickly. The core top descended from its maximum height to its minimum height in only 4.0–10.5 min (Fig. 15).

All downbursts also contained similar patterns of midlevel convergence magnitude. The magnitude increased to a peak as the core top and bottom descended and then decreased as the core depth, and potentially the downdraft depth, decreased (Figs. 7a, 9a, 11a, and 13a). The midlevel convergence size evolved similarly for the three severe downbursts. It increased as the core bottom or top descended and then decreased as the core depth decreased (Figs. 7b, 9b, 11b, and 13b). Conversely, the midlevel convergence size remained relatively constant for the nonsevere downburst despite the descent of the reflectivity core and changes in the midlevel convergence magnitude (Figs. 13 and 16). While it is unclear why this pattern exists for NSD-a, similar patterns in midlevel convergence size may provide an indication of downburst severity. A larger sample size is needed to draw any conclusions about midlevel convergence size and its potential relationship to downburst severity.

Changes in midlevel convergence magnitude and size occurred over very short time scales, with increasing convergence magnitude persisting for 8 min or less (Fig. 16a) and increasing convergence size persisting for 9 min or less (Fig. 16b). Conventional volumetric update times could easily undersample this increasing trend. Peak midlevel convergence magnitude could also occur between conventional volume scans, especially if it evolves as quickly as that observed with SD-a (Fig. 7a).

It was important to sample these rapidly evolving signatures because they provided a signal for downburst intensification on 14 June 2011. The increasing and peak midlevel convergence magnitudes occurred on average 9.4 and 4.6 min prior to the downburst maximum intensity, respectively, while the increasing and peak midlevel convergence sizes occurred on average 5.2 and 13.0 min prior to the downburst maximum intensity,

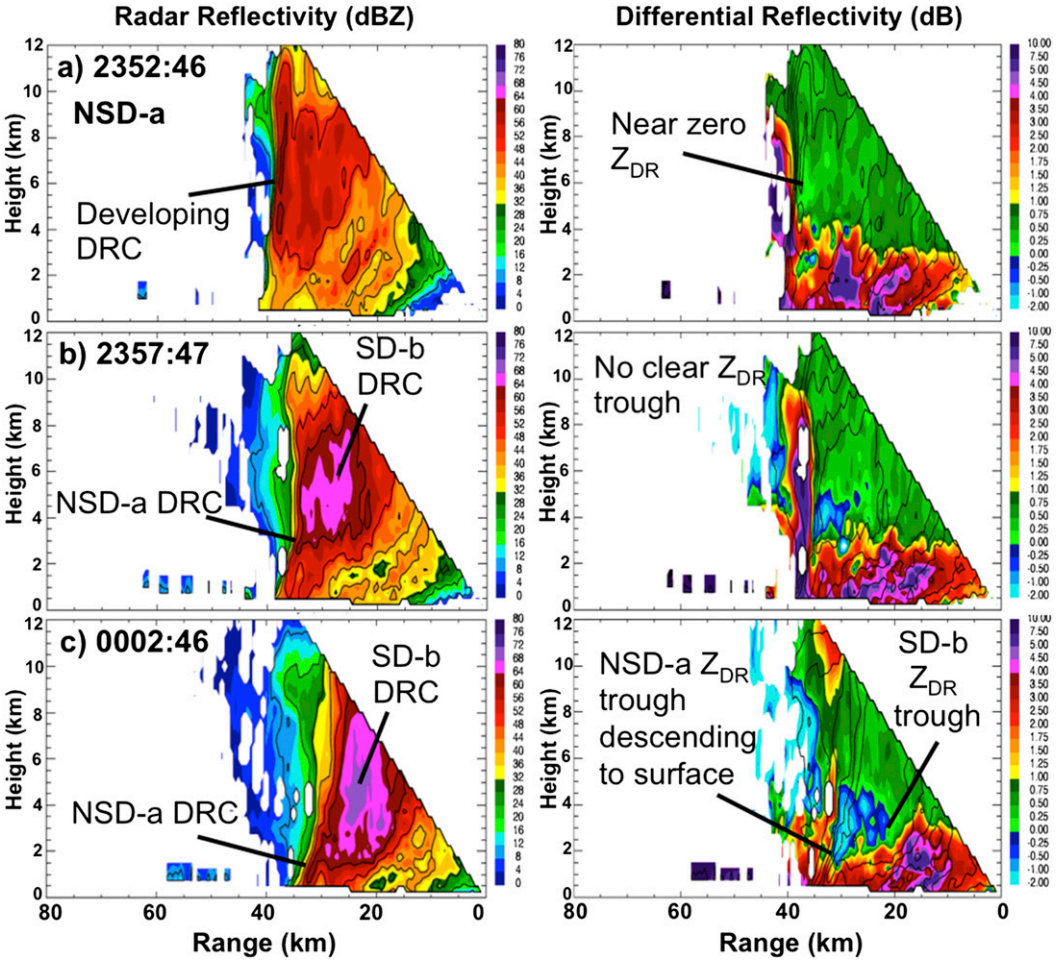

FIG. 14. As in Fig. 8, but for NSD-a at (a) 2352:46, (b) 2357:47, and (c) 0002:46 UTC 14–15 Jun 2011. SD-b's unrelated DRC is also noted. Azimuths are 273°, 275°, and 278°, respectively.

respectively (Table 4). Both severe and nonsevere downbursts did display similar trends and magnitudes of midlevel convergence, which limited the ability to predict downburst intensity (i.e., nonsevere or severe) in this case. This result does differ from that of Isaminger (1988), who found a relationship between midlevel convergence magnitude and downburst intensity. Therefore, a larger sample size that includes a wide range of downburst intensities and null events is needed to address the potential relationship between midlevel convergence magnitude and downburst intensity. It is also important to examine the midlevel convergence size because evolutionary patterns were different between severe and nonsevere downbursts in this case. In addition, Smith et al. (2004) found that midlevel convergence size could be an important signature for anticipating downburst development.

Slow volumetric update times—similar to those of the current WSR-88D network—limited our ability to quantify trends and time scales associated with dual-polarization precursors. For example, the Z_{DR} trough of SD-b descended from near 2.5 km ARL to near the surface in only one volume scan (Figs. 10b,c), while the Z_{DR} trough of NSD-a was only sampled by one KOUN volume scan (Fig. 14c). Rapid-update dual-polarization data are needed to observe potentially useful trends in these signatures. For example, trends in the descent and depth of the Z_{DR} trough could provide useful information about downburst development and intensification (e.g., Scharfenberg 2003; Ryzhkov et al. 2013a). More frequent updates showing the detailed evolution of microphysical fingerprints (e.g., melting; Kumjian 2012) could also point to DRCs that have an increased downburst potential due to additional cooling via melting. With the slower update time of KOUN, dual-polarization data in this case provided limited trend information about hydrometeor type and downdraft location compared to the more detailed evolution

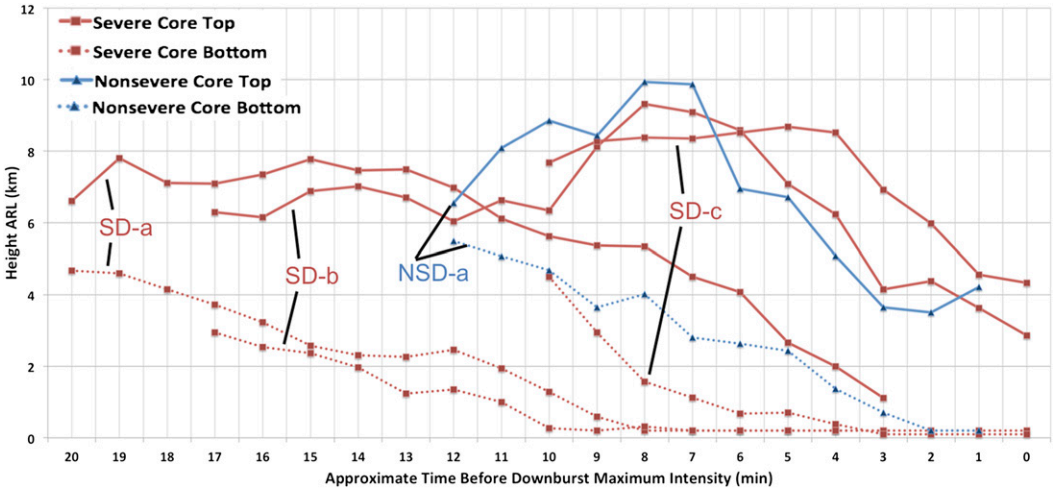

FIG. 15. Evolution of the DRC for all analyzed severe (red lines) and nonsevere (blue line) downbursts on 14 Jun 2011. Solid lines show the core top and dashed lines the core bottom.

of traditional precursors (e.g., DRCs) observed by PAR. For all downbursts, dual-polarization variables indicated that hail was likely present in their reflectivity cores. This hail increased the potential for hydrometeor loading and melting, which could result in a stronger downburst (e.g., Straka and Anderson 1993; Richter et al. 2014). In this study, Z_{DR} troughs were observed with all examined downbursts. They first appeared as the PAR-observed reflectivity core bottom descended below the in-storm melting layer. Then, the core bottom and the Z_{DR} trough descended and reached near the surface close to the time of downburst development, which was similar to the observations by Wakimoto and Bringi (1988). Hereafter, the Z_{DR} trough persisted as the core top descended toward the surface, and then dissipated as the reflectivity core dissipated.

b. Operational implications

The rapidly evolving precursor signatures observed on 14 June 2011 help to explain some of the WSR-88D's limitations identified by LaDue et al. (2010). Without rapid-update radar data, forecasters are less able to observe and use precursor signatures and therefore rely on environmental cues and near-surface divergent signatures to diagnose downburst potential (LaDue et al. 2010; M. Austin, NWS Forecast Office Norman, 2015, personal communication). The results of this case suggest that rapid-update radar data may provide valuable information about wet downburst precursor signatures to forecasters, at least in instances with similar environments and storm characteristics. Specifically, trends in precursor evolution may provide reliable signals that a downburst is about to develop. Therefore, providing automatically computed trends (e.g., Fig. 7) to forecasters in real time, when rapid-update data become available, may aid in their ability to anticipate downburst intensification. For example, downburst maximum intensity was preceded by rapid descent of the core top and increasing midlevel convergence magnitude by at least 4.2 min in this case (Table 3).

Results indicate that the ability to sample the short-lived trends in midlevel convergence magnitude and size observed here (Figs. 15 and 16) may aid a forecaster in attempting to discern the intensity of an impending downburst. For example, midlevel convergence size followed a distinct pattern of increasing to a peak value before decreasing as the core depth decreased for all severe downbursts in this case (Fig. 16). This pattern was not observed for the nonsevere downburst, as midlevel convergence size remained almost constant during DRC

TABLE 3. Overview of time differences (delta T; min) between the descent of the core top and the downburst maximum intensity (first two columns) and DRC and increasing midlevel convergence magnitude/size (delta T for size in parentheses) occurring together and downburst maximum intensity (third and fourth columns) for all analyzed downbursts on 14 Jun 2011.

DRC top descent		DRC and evidence of increasing convergence magnitude (size)	
Downburst	Delta T	Downburst	Delta T
SD-a	13.6	SD-a	13.6 (13.6)
SD-b	8.8	SD-b	5.6 (7.7)
SD-c	4.2	SD-c	4.2 (4.2)
NSD-a	7.9	NSD-a	5.8 (N/A)
Avg	8.6	Avg	7.3 (8.5)

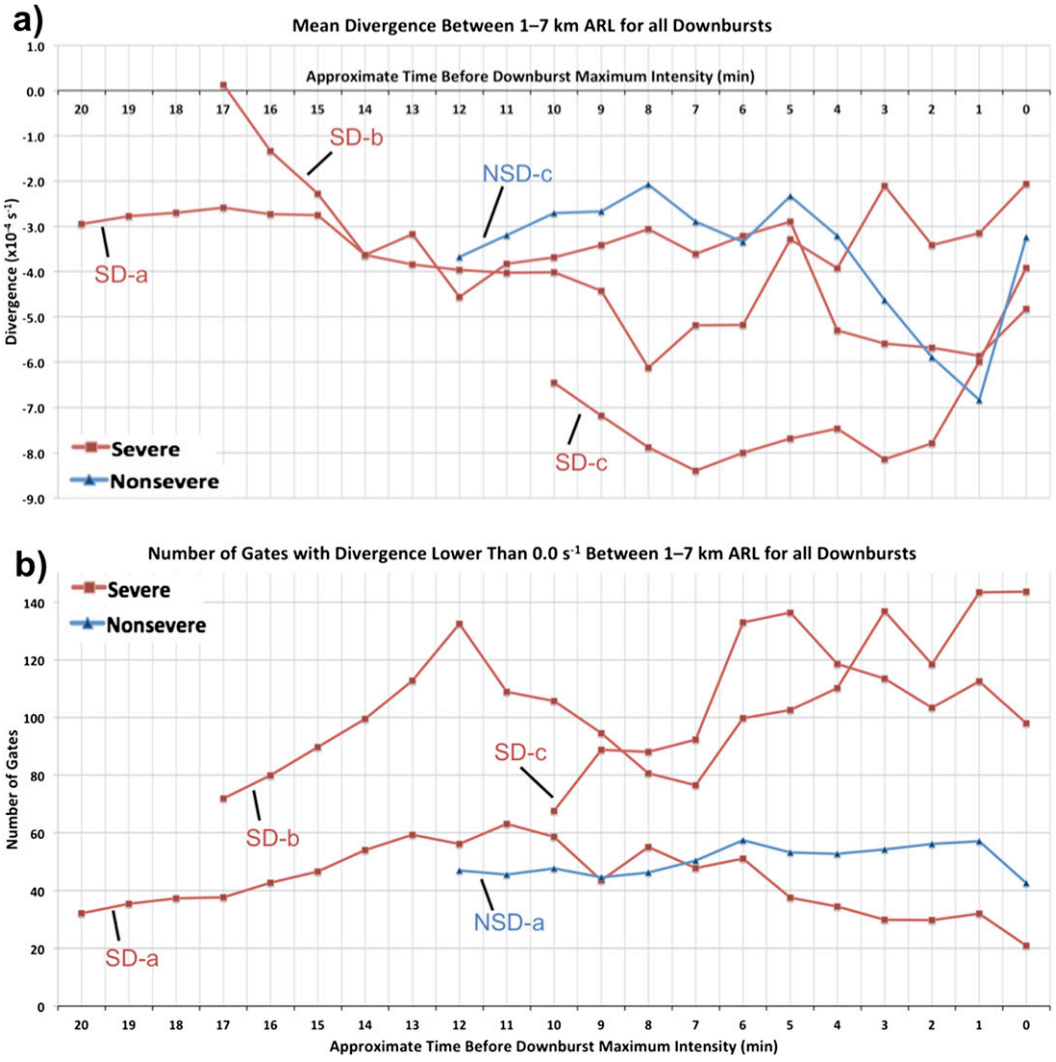

FIG. 16. Evolution of (a) mean midlevel convergence and (b) number of gates with divergence lower than 0.0 s^{-1} (i.e., convergence size) between 1.0 (1.5)–7.0 km ARL for all analyzed severe (red lines) and nonsevere (blue line) downbursts on 14 Jun 2011. In (a), negative divergence is convergence.

evolution. Based on results from Isaminger (1988) and analysis of PAR data from another downburst event occurring on 10 July 2013 (Kuster 2014), midlevel convergence magnitude may also provide information about the potential severity of an impending downburst.

Dual-polarization data could help a forecaster identify reflectivity cores containing hail, which pose greater downburst potential as a result of hydrometeor loading and cooling if the hail melts (e.g., Srivastava 1987; Proctor 1989; Richter et al. 2014). The development of Z_{DR} troughs could also increase a forecaster's confidence in the presence of a downdraft and the potential for hail or high winds at the surface (e.g., Wakimoto and Bringi 1988; Zrnić et al. 1993; Ryzhkov et al. 2013a). The presence of a Z_{DR} trough may not provide information about the potential for downburst intensity (i.e., severe or nonsevere) however, since they were observed with all analyzed downbursts on 14 June 2011, regardless of their intensity. It is possible that rapid-update data provided by a future dual-polarization PAR (e.g., Zhang et al. 2009, 2011) could reveal key details about trends in dual-polarization signatures—similar to those presented in Ryzhkov et al. (2013a) and Kumjian et al. (2014)—that could aid forecasters in anticipating downburst development and intensity.

7. Summary

This study used rapid-update PAR data to examine downburst precursor signatures within an intense

TABLE 4. Overview of time differences (delta T; min) between the peak in midlevel convergence magnitude/size (delta T for size in parentheses) and downburst maximum intensity (first two columns) and increasing midlevel convergence magnitude/size and downburst maximum intensity (third and fourth columns) for all analyzed downbursts on 14 Jun 2011. Negative delta T indicates that the precursor signature occurred after the downburst maximum intensity.

Max midlevel convergence magnitude (size)		Increasing midlevel convergence magnitude (size)	
Downburst	Delta T	Downburst	Delta T
SD-a	8.4 (11.5)	SD-a	15.7 (20.8)
SD-b	1.1 (−1.5)	SD-b	5.6 (7.7)
SD-c	7.3 (5.23)	SD-c	10.5 (10.5)
NSD-a	1.6 (N/A)	NSD-a	5.8 (N/A)
Avg	4.6 (5.2)	Avg	9.4 (13.0)

multicell thunderstorm in central Oklahoma. Through an analysis of three severe downbursts and one nonsevere downburst we observed the following:

1) the collapse of the core top occurred 4.2–13.6 min prior to the downburst maximum intensity and appeared to be associated with downburst intensification,
2) the midlevel convergence increased to a peak magnitude in 8 min or less as the core top and bottom descended and then decreased as the core depth decreased,
3) the pattern of midlevel convergence size typically contained large changes and clear maxima for severe downbursts, but contained very few changes and no clear maximum for the nonsevere downburst,
4) Z_{DR} troughs occurred with all downbursts and descended, along with the core bottom observed by PAR, to the lowest elevation angle, and
5) rapid-update radar data were required to adequately sample the downburst precursor signature trends since they evolved very rapidly (generally in less than 10 min).

Ultimately, the ability to observe these key features in a forecaster's downburst conceptual model could increase confidence in issuing warnings for damaging winds caused by downbursts (Bowden et al. 2015).

All downbursts displayed similar DRC and midlevel convergence magnitude patterns regardless of intensity in this case (Figs. 15 and 16a). The small sample size, narrow range of downburst intensities considered (i.e., all downbursts had similar maximum base velocity and DeltaV), and challenges in accurately classifying downbursts as severe or nonsevere—primarily due to issues with *Storm Data* (e.g., Doswell et al. 2005; Trapp et al. 2006)—likely limited our ability to comment on differences between severe and nonsevere downburst precursors. Based on previous work by Isaminger (1988), Kuster (2014), and the differences observed in the midlevel convergence sizes here, we infer that midlevel convergence could be a good focus for future research. An increase in sample size, with PAR-like volumetric update times, of downbursts with varying intensities across multiple geographic regions could show differences in midlevel convergence or other precursors that could reliably indicate an impending downburst's likelihood of reaching severe limits. Future work using rapid-update dual-polarization data could also reveal important information about trends in signatures such as Z_{DR} troughs.

Acknowledgments. The authors thank Jeff Brogden, Karen Cooper, and Robert Toomey for their expertise with WDSSII; Michael Biggerstaff and Phillip Chilson for their input and guidance; Eddie Forren, Richard Adams, Dave Priegnitz, and John Krause for their help with radar data processing; Emma Kuster and Tim Supinie for assistance with Python; and Kurt Hondl and Don Burgess for their internal reviews of the manuscript. We also thank three anonymous reviewers who helped us clarify and strengthen the manuscript. Funding for the lead author was provided by NOAA/Office of Oceanic and Atmospheric Research under NOAA–University of Oklahoma Cooperative Agreement NA11OAR4320072, U.S. Department of Commerce.

REFERENCES

Atkins, N. T., and R. M. Wakimoto, 1991: Wet microburst activity over the southeastern United States: Implications for forecasting. *Wea. Forecasting*, **6**, 470–482, doi:10.1175/1520-0434(1991)006<0470:WMAOTS>2.0.CO;2.

Battan, L. J., and J. B. Theiss, 1966: Observations of vertical motions and particle sizes in a thunderstorm. *J. Atmos. Sci.*, **23**, 78–87, doi:10.1175/1520-0469(1966)023<0078:OOVMAP>2.0.CO;2.

Bowden, K. A., P. L. Heinselman, D. M. Kingfield, and R. P. Thomas, 2015: Impacts of phased-array radar data on forecaster performance during severe hail and wind events. *Wea. Forecasting*, **30**, 389–404, doi:10.1175/WAF-D-14-00101.1.

Brandes, E. A., J. Vivekanandan, and J. D. Tuttle, 1995: A study of thunderstorm microphysics with multiparameter radar and aircraft observations. *Mon. Wea. Rev.*, **123**, 3129–3143, doi:10.1175/1520-0493(1995)123<3129:ASOTMW>2.0.CO;2.

Bringi, V. N., T. A. Seliga, and K. Aydin, 1984: Hail detection with a differential reflectivity radar. *Science*, **225**, 1145–1147, doi:10.1126/science.225.4667.1145.

——, J. Vivekanandan, and J. D. Tuttle, 1986: Multiparameter radar measurements in Colorado convective storms. Part II: Hail detection studies. *J. Atmos. Sci.*, **43**, 2564–2577, doi:10.1175/1520-0469(1986)043<2564:MRMICC>2.0.CO;2.

Brown, R. A., and V. T. Wood, 2000: Improved WSR-88D scanning strategies for convective storms. *Wea. Forecasting*, **15**, 208–220, doi:10.1175/1520-0434(2000)015<0208:IWSSFC>2.0.CO;2.

——, R. M. Steadham, B. A. Flickinger, R. R. Lee, D. Sirmans, and V. T. Wood, 2005: New WSR-88D volume coverage pattern

12: Results of field tests. *Wea. Forecasting*, **20**, 385–393, doi:10.1175/WAF848.1.

Caracena, F., J. McCarthy, and J. A. Flueck, 1983: Forecasting the likelihood of microbursts along the Front Range of Colorado. Preprints, *13th Conf. on Severe Local Storms*, Tulsa, OK, Amer. Meteor. Soc., 261–264.

Caylor, I. C., and A. J. Illingworth, 1987: Radar observations and modeling of warm rain initiation. *Quart. J. Roy. Meteor. Soc.*, **113**, 1171–1191, doi:10.1002/qj.49711347806.

Chandrasekar, V., R. Keränen, and D. Moisseev, 2013: Recent advances in classification of observations from dual polarization weather radars. *Atmos. Res.*, **119**, 97–111, doi:10.1016/j.atmosres.2011.08.014.

Doswell, C. A., III, D. W. Burgess, and M. P. Kay, 2005: Climatological estimates of daily local nontornadic severe thunderstorm probability for the United States. *Wea. Forecasting*, **20**, 577–595, doi:10.1175/WAF866.1.

Eilts, M. D., 1987: Low altitude wind shear detection with Doppler radar. *J. Climate Appl. Meteor.*, **26**, 96–106, doi:10.1175/1520-0450(1987)026<0096:LAWSDW>2.0.CO;2.

——, and R. J. Doviak, 1987: Oklahoma downbursts and their asymmetry. *J. Climate Appl. Meteor.*, **26**, 69–78, doi:10.1175/1520-0450(1987)026<0069:ODATA>2.0.CO;2.

——, J. T. Johnson, E. D. Mitchell, R. J. Lynn, P. Spencer, S. Cobb, and T. M. Smith, 1996: Damaging downburst prediction and detection algorithm for the WSR-88D. Preprints, *18th Conf. on Severe Local Storms*, San Francisco, CA, Amer. Meteor. Soc., 541–545.

Ellrod, G. P., 1989: Environmental conditions associated with the Dallas microburst storm determined from satellite soundings. *Wea. Forecasting*, **4**, 469–484, doi:10.1175/1520-0434(1989)004<0469:ECAWTD>2.0.CO;2.

Fawbush, E. J., and R. C. Miller, 1953: A method for forecasting hailstone size at the earth's surface. *Bull. Amer. Meteor. Soc.*, **34**, 235–244.

Forsyth, D. E., and Coauthors, 2005: The National Weather Radar Testbed (phased-array). Preprints, *32nd Conf. on Radar Meteorology*, Albuquerque, NM, Amer. Meteor. Soc., 12R.3. [Available at https://ams.confex.com/ams/32Rad11Meso/techprogram/paper_96377.htm.]

Fujita, T. T., and H. R. Byers, 1977: Spearhead echo and downburst in the crash of an airliner. *Mon. Wea. Rev.*, **105**, 129–146, doi:10.1175/1520-0493(1977)105<0129:SEADIT>2.0.CO;2.

——, and R. M. Wakimoto, 1983: Microbursts in JAWS depicted by Doppler radars, PAM, and aerial photographs. Preprints, *21st Conf. on Radar Meteorology*, Edmonton, AB, Canada, Amer. Meteor. Soc., 638–645.

Giangrande, S. E., J. M. Krause, and A. V. Ryzhkov, 2008: Automatic designation of the melting layer with a polarimetric prototype of the WSR-88D radar. *J. Appl. Meteor. Climatol.*, **47**, 1354–1364, doi:10.1175/2007JAMC1634.1.

Hall, M. P. M., J. W. F. Goddard, and S. M. Cherry, 1984: Identification of hydrometeors and other targets by dual-polarization radar. *Radio Sci.*, **19**, 132–140, doi:10.1029/RS019i001p00132.

Heinselman, P. L., and S. M. Torres, 2011: High-temporal-resolution capabilities of the National Weather Radar Testbed Phased-Array Radar. *J. Appl. Meteor. Climatol.*, **50**, 579–593, doi:10.1175/2010JAMC2588.1.

——, D. L. Priegnitz, K. L. Manross, T. M. Smith, and R. W. Adams, 2008: Rapid sampling of severe storms by the National Weather Radar Testbed Phased Array Radar. *Wea. Forecasting*, **23**, 808–824, doi:10.1175/2008WAF2007071.1.

Herzegh, P. H., and A. R. Jameson, 1992: Observing precipitation through dual-polarization radar measurements. *Bull. Amer. Meteor. Soc.*, **73**, 1365–1374, doi:10.1175/1520-0477(1992)073<1365:OPTDPR>2.0.CO;2.

Hjelmfelt, M. R., 1987: The microbursts of 22 June 1982 in JAWS. *J. Atmos. Sci.*, **44**, 1646–1665, doi:10.1175/1520-0469(1987)044<1646:TMOJIJ>2.0.CO;2.

Isaminger, M. A., 1988: A preliminary study of precursors to Huntsville microbursts. Lincoln Laboratory Project Rep. ATC-153, 22 pp. [Available online at https://www.ll.mit.edu/mission/aviation/publications/publication-files/atc-reports/Isaminger_1988_ATC-153-WW-15318.pdf.]

Jewell, R., and J. Brimelow, 2009: Evaluation of Alberta hail growth model using severe hail proximity soundings from the United States. *Wea. Forecasting*, **24**, 1592–1609, doi:10.1175/2009WAF2222230.1.

Kessinger, C. J., D. B. Parsons, and J. W. Wilson, 1988: Observations of a storm containing misocyclones, downbursts, and horizontal vortex circulations. *Mon. Wea. Rev.*, **116**, 1959–1982, doi:10.1175/1520-0493(1988)116<1959:OOASCM>2.0.CO;2.

Knupp, K. R., 1996: Structure and evolution of a long-lived, microburst-producing storm. *Mon. Wea. Rev.*, **124**, 2785–2806, doi:10.1175/1520-0493(1996)124<2785:SAEOAL>2.0.CO;2.

Kumjian, M. R., 2012: The impact of precipitation physical processes on the polarimetric radar variables. Ph.D. dissertation, University of Oklahoma, 327 pp. [Available online at http://gradworks.umi.com/35/07/3507433.html.]

——, 2013: Principles and applications of dual-polarization weather radar. Part I: Description of the polarimetric radar variables. *J. Oper. Meteor.*, **1**, 226–264, doi:10.15191/nwajom.2013.0119.

——, and A. V. Ryzhkov, 2008: Polarimetric signatures in supercell thunderstorms. *J. Appl. Meteor. Climatol.*, **47**, 1940–1961, doi:10.1175/2007JAMC1874.1.

——, A. Khain, N. Benmoshe, E. Ilotoviz, A. V. Ryzhkov, and V. T. J. Phillips, 2014: The anatomy and physics of Z_{DR} columns: Investigating a polarimetric radar signature with a spectral bin microphysical model. *J. Appl. Meteor. Climatol.*, **53**, 1820–1843, doi:10.1175/JAMC-D-13-0354.1.

Kuster, C. M., 2014: Non-traditional radar observations of downbursts. M.S. thesis, School of Meteorology, University of Oklahoma, 128 pp.

LaDue, D. S., P. L. Heinselman, and J. F. Newman, 2010: Strengths and limitations of current radar systems for two stakeholder groups in the southern plains. *Bull. Amer. Meteor. Soc.*, **91**, 899–910, doi:10.1175/2009BAMS2830.1.

Mahale, V. N., G. Zhang, and M. Zue, 2013: The microphysics of the 14 June 2011 Norman, Oklahoma, downburst from dual-polarization and dual-Doppler radar measurements. *Proc. 16th Conf. on Aviation, Range, and Aerospace Meteorology*, Austin, TX, Amer. Meteor. Soc., 5.1. [Available online at https://ams.confex.com/ams/93Annual/webprogram/Paper216605.html.]

McCarthy, J., J. W. Wilson, and T. T. Fujita, 1982: The Joint Airport Weather Studies (JAWS) project. *Bull. Amer. Meteor. Soc.*, **63**, 15–22, doi:10.1175/1520-0477(1982)063<0015:TJAWSP>2.0.CO;2.

NCDC, 2011: Storm Events Database. [Available online at http://www.ncdc.noaa.gov/stormevents.]

Nelson, S. P., 1983: The influence of storm flow structure on hail growth. *J. Atmos. Sci.*, **40**, 1965–1983, doi:10.1175/1520-0469(1983)040<1965:TIOSFS>2.0.CO;2.

——, 1987: The hybrid multicellular–supercellular storm—An efficient hail producer. Part II: General characteristics and implications for hail growth. *J. Atmos. Sci.*, **44**, 2060–2073, doi:10.1175/1520-0469(1987)044<2060:THMSEH>2.0.CO;2.

Newman, J. F., and P. L. Heinselman, 2012: Evolution of a quasi-linear convective system sampled by phased array radar. *Mon. Wea. Rev.*, **140**, 3467–3486, doi:10.1175/MWR-D-12-00003.1.

——, V. Lakshmanan, P. L. Heinselman, M. B. Richman, and T. M. Smith, 2013: Range-correcting azimuthal shear in Doppler radar data. *Wea. Forecasting*, **28**, 194–211, doi:10.1175/WAF-D-11-00154.1.

Peterson, R. E., Jr., 1984: A triple-Doppler radar analysis of a discretely propagating multicell convective storm. *J. Atmos. Sci.*, **41**, 2973–2990, doi:10.1175/1520-0469(1984)041<2973:ATDRAO>2.0.CO;2.

Picca, J. C., M. R. Kumjian, and A. V. Ryzhkov, 2010: Z_{DR} columns as a predictive tool for hail growth and storm evaluation. *Proc. 25th Conf. on Severe Local Storms*, Denver, CO, Amer Meteor. Soc., 11.3. [Available online at https://ams.confex.com/ams/25SLS/webprogram/Paper175750.html.]

Proctor, F. H., 1988: Numerical simulations of an isolated microburst. Part I: Dynamics and structure. *J. Atmos. Sci.*, **45**, 3137–3160, doi:10.1175/1520-0469(1988)045<3137:NSOAIM>2.0.CO;2.

——, 1989: Numerical simulations of an isolated microburst. Part II: Sensitivity experiments. *J. Atmos. Sci.*, **46**, 2143–2165, doi:10.1175/1520-0469(1989)046<2143:NSOAIM>2.0.CO;2.

Richter, H., J. Peter, and S. Collis, 2014: Analysis of a destructive wind storm on 16 November 2008 in Brisbane, Australia. *Mon. Wea. Rev.*, **142**, 3038–3060, doi:10.1175/MWR-D-13-00405.1.

Roberts, R. D., and J. W. Wilson, 1989: A proposed microburst nowcasting procedure using single-Doppler radar. *J. Appl. Meteor.*, **28**, 285–303, doi:10.1175/1520-0450(1989)028<0285:APMNPU>2.0.CO;2.

Ryzhkov, A. V., T. J. Schuur, D. W. Burgess, P. L. Heinselman, S. E. Giangrande, and D. S. Zrnić, 2005: The Joint Polarization Experiment: Polarimetric rainfall measurements and hydrometeor classification. *Bull. Amer. Meteor. Soc.*, **86**, 809–824, doi:10.1175/BAMS-86-6-809.

——, M. R. Kumjian, S. M. Ganson, and A. P. Khain, 2013a: Polarimetric radar characteristics of melting hail. Part I: Theoretical simulations using spectral microphysical modeling. *J. Appl. Meteor. Climatol.*, **52**, 2849–2870, doi:10.1175/JAMC-D-13-073.1.

——, ——, ——, and P. Zhang, 2013b: Polarimetric radar characteristics of melting hail. Part II: Practical implications. *J. Appl. Meteor. Climatol.*, **52**, 2871–2886, doi:10.1175/JAMC-D-13-074.1.

Scharfenberg, K. A., 2003: Polarimetric radar signatures in microburst-producing thunderstorms. Preprints, *31st Int. Conf. on Radar Meteorology*, Seattle, WA, Amer. Meteor. Soc., 8B.4. [Available online at https://ams.confex.com/ams/32BC31R5C/techprogram/paper_64413.htm.]

Schmocker, G. K., R. W. Przybylinski, and Y.-J. Lin, 1996: Forecasting the initial onset of damaging downburst winds associated with a mesoscale convective system (MCS) using the mid-altitude radial convergence (MARC) signature. Preprints, *15th Conf. on Weather Analysis and Forecasting*, Norfolk, VA, Amer. Meteor. Soc., 306–311.

Smith, T. M., and K. L. Elmore, 2004: The use of radial velocity derivative to diagnose rotation and divergence. Preprints, *11th Conf. on Aviation, Range, and Aerospace*, Hyannis, MA, Amer. Meteor. Soc., P5.6. [Available online at https://ams.confex.com/ams/pdfpapers/81827.pdf.]

——, ——, and S. A. Dulin, 2004: A damaging downburst prediction and detection algorithm for the WSR-88D. *Wea. Forecasting*, **19**, 240–250, doi:10.1175/1520-0434(2004)019<0240:ADDPAD>2.0.CO;2.

Srivastava, R. C., 1985: A simple model of evaporatively driven downdraft: Application to microburst downdraft. *J. Atmos. Sci.*, **42**, 1004–1023, doi:10.1175/1520-0469(1985)042<1004:ASMOED>2.0.CO;2.

——, 1987: A model of intense downdrafts driven by the melting and evaporation of precipitation. *J. Atmos. Sci.*, **44**, 1752–1774, doi:10.1175/1520-0469(1987)044<1752:AMOIDD>2.0.CO;2.

Straka, J. M., and J. R. Anderson, 1993: Numerical simulations of microburst-producing storms: Some results from storms observed during COHMEX. *J. Atmos. Sci.*, **50**, 1329–1348, doi:10.1175/1520-0469(1993)050<1329:NSOMPS>2.0.CO;2.

——, D. S. Zrnić, and A. V. Ryzhkov, 2000: Bulk hydrometeor classification and quantification using polarimetric radar data: Synthesis of relations. *J. Appl. Meteor.*, **39**, 1341–1372, doi:10.1175/1520-0450(2000)039<1341:BHCAQU>2.0.CO;2.

Trapp, R. J., D. M. Wheatley, N. T. Atkins, R. W. Przybylinski, and R. Wolf, 2006: Buyer beware: Some words of caution on the use of severe wind reports in postevent assessment and research. *Wea. Forecasting*, **21**, 408–415, doi:10.1175/WAF925.1.

Vasiloff, S. V., and K. W. Howard, 2009: Investigation of a severe downburst storm near Phoenix, Arizona, as seen by a mobile Doppler radar and the KIWA WSR-88D. *Wea. Forecasting*, **24**, 856–867, doi:10.1175/2008WAF2222117.1.

Wakimoto, R. M., 1985: Forecasting dry microburst activity over the high plains. *Mon. Wea. Rev.*, **113**, 1131–1143, doi:10.1175/1520-0493(1985)113<1131:FDMAOT>2.0.CO;2.

——, 2001: Convectively driven high wind events. *Severe Convective Storms*, *Meteor. Monogr.*, No. 50. Amer. Meteor. Soc., 255–298.

——, and V. N. Bringi, 1988: Dual-polarization observations of microbursts associated with intense convection: The 20 July storm during the MIST project. *Mon. Wea. Rev.*, **116**, 1521–1539, doi:10.1175/1520-0493(1988)116<1521:DPOOMA>2.0.CO;2.

Willingham, K. M., E. J. Thompson, K. W. Howard, and C. L. Dempsey, 2011: Characteristics of Sonoran Desert microbursts. *Wea. Forecasting*, **26**, 94–108, doi:10.1175/2010WAF2222388.1.

Wilson, J. W., and D. Reum, 1986: The hail spike: Reflectivity and velocity signature. Preprints, *23rd Conf. on Radar Meteorology*, Snowmass, CO, Amer. Meteor. Soc., 62–65.

——, R. D. Roberts, C. Kessinger, and J. McCarthy, 1984: Microburst wind structure and evaluation of Doppler radar for airport wind shear detection. *J. Climate Appl. Meteor.*, **23**, 898–915, doi:10.1175/1520-0450(1984)023<0898:MWSAEO>2.0.CO;2.

Zhang, G., R. J. Doviak, D. S. Zrnić, J. E. Crain, D. Staiman, and Y. Al-Rashid, 2009: Phased array radar polarimetry for weather sensing: A theoretical formulation for polarization calibration. *IEEE Trans. Geosci. Remote Sens.*, **47**, 3679–3689, doi:10.1109/TGRS.2009.2029332.

——, ——, ——, R. Palmer, L. Lei, and Y. Al-Rashid, 2011: Polarimetric phased-array radar for weather measurement: A planar or cylindrical configuration? *J. Atmos. Oceanic Technol.*, **28**, 63–73, doi:10.1175/2010JTECHA1470.1.

Zrnić, D. S., V. N. Bringi, N. Balakrishnan, K. Aydin, V. Chandrasekar, and J. Hubbert, 1993: Polarimetric measurements in a severe hailstorm. *Mon. Wea. Rev.*, **121**, 2223–2238, doi:10.1175/1520-0493(1993)121<2223:PMIASH>2.0.CO;2.

——, and Coauthors, 2007: Agile-beam phased array radar for weather observations. *Bull. Amer. Meteor. Soc.*, **88**, 1753–1766, doi:10.1175/BAMS-88-11-1753.